ANTIOXIDANTS & REDOX SIGNALING
Volume 21, Number 4, 2014

DOI: 10.1089/ars.2013.5696

FORUM ORIGINAL RESEARCH COMMUNICATION

S-Nitrosoglutathione Reductase Deficiency-Induced *S*-Nitrosylation Results in Neuromuscular Dysfunction

Costanza Montagna,[1,*] Giuseppina Di Giacomo,[1,*] Salvatore Rizza,[2,3] Simone Cardaci,[2,†] Elisabetta Ferraro,[1] Paolo Grumati,[4] Daniela De Zio,[2,5] Emiliano Maiani,[2,3] Carolina Muscoli,[6,7] Filomena Lauro,[6,7] Sara Ilari,[6,7] Sergio Bernardini,[2] Stefano Cannata,[2] Cesare Gargioli,[8] Maria R. Ciriolo,[1,2] Francesco Cecconi,[2,3,5] Paolo Bonaldo,[4] and Giuseppe Filomeni[1–3]

Abstract

Aims: Nitric oxide (NO) production is implicated in muscle contraction, growth and atrophy, and in the onset of neuropathy. However, many aspects of the mechanism of action of NO are not yet clarified, mainly regarding its role in muscle wasting. Notably, whether NO production-associated neuromuscular atrophy depends on tyrosine nitration or *S*-nitrosothiols (SNOs) formation is still a matter of debate. Here, we aim at assessing this issue by characterizing the neuromuscular phenotype of *S*-nitrosoglutathione reductase-null (GSNOR-KO) mice that maintain the capability to produce NO, but are unable to reduce SNOs. ***Results:*** We demonstrate that, without any sign of protein nitration, young GSNOR-KO mice show neuromuscular atrophy due to loss of muscle mass, reduced fiber size, and neuropathic behavior. In particular, GSNOR-KO mice show a significant decrease in nerve axon number, with the myelin sheath appearing disorganized and reduced, leading to a dramatic development of a neuropathic phenotype. Mitochondria appear fragmented and depolarized in GSNOR-KO myofibers and myotubes, conditions that are reverted by *N*-acetylcysteine treatment. Nevertheless, although atrogene transcription is induced, and bulk autophagy activated, no removal of damaged mitochondria is observed. These events, alongside basal increase of apoptotic markers, contribute to persistence of a neuropathic and myopathic state. ***Innovation:*** Our study provides the first evidence that GSNOR deficiency, which affects exclusively SNOs reduction without altering nitrotyrosine levels, results in a clinically relevant neuromuscular phenotype. ***Conclusion:*** These findings provide novel insights into the involvement of GSNOR and *S*-nitrosylation in neuromuscular atrophy and neuropathic pain that are associated with pathological states; for example, diabetes and cancer. *Antioxid. Redox Signal*. 21, 570–587.

Introduction

NITRIC OXIDE (NO) production by neuronal NO synthase (nNOS) has been implicated in a plethora of physiopathological processes involving the neuromuscular apparatus. Due to NO being a pleiotropic molecule, it can elicit several signaling pathways required for correct muscle contraction (56) and hypertrophy induced by overloading (54), or, paradoxically, for mediating atrophy (21, 56, 61). Regarding this last issue, it is still a matter of debate as to how NO negatively affects neuromuscular function.

Besides the well-documented ability to bind heme iron (Fe-nitrosylation) (38), NO can react with reactive oxygen species (ROS), generating more dangerous reactive nitrogen

[1]Research Center, IRCCS San Raffaele Pisana, Rome, Italy.
[2]Department of Biology, University of Rome ''Tor Vergata,'' Rome, Italy.
[3]Cell Stress and Survival Unit, Danish Cancer Society Research Center, Copenhagen, Denmark.
[4]Department of Biomedical Sciences, University of Padua, Padua, Italy.
[5]IRCCS Fondazione Santa Lucia, Rome, Italy.
[6]Department of Life Science, University of Catanzaro ''Magna Graecia,'' Catanzaro, Italy.
[7]Centro del Farmaco, IRCCS San Raffaele Pisana, Rome, Italy.
[8]IRCCS MultiMedica, Milan, Italy.
*These authors equally contributed to this work and should be considered first co-authors.
†*Current affiliation:* Cancer Research UK, The Beatson Institute for Cancer Research, Glasgow, United Kingdom.

Innovation

The detrimental role of NO overproduction in neuromuscular function is well documented; however, due to the nature of the experimental system used, it is still a matter of debate whether this mainly depends on nitroxidative damage or *S*-nitrosylation. Here, we provide the first *in vivo* evidence that the genetic ablation of *GSNOR*, which affects exclusively nitrosothiol reduction without altering nitrotyrosine levels, results in a clinically relevant neuromuscular phenotype resembling neuropathic pain-associated muscle atrophy. Our results indicate that *S*-nitrosoglutathione reductase (GSNOR) and nitrosative stress could represent elective targets for denitrosylating agent-based therapies.

species (*e.g.*, peroxynitrite, $ONOO^-$), that can affect protein structure and function (21). Tyrosine nitration is one of the main modifications occurring under conditions of NO overproduction, and it mostly depends on the ability of $ONOO^-$ to catalyze the addition of a nitro group (NO_2) to the aromatic ring in tyrosine residues (7, 26). The accumulation of protein nitrotyrosines is commonly used as a pathological marker of proteins subjected to excessive nitroxidative stress (6, 55) and has been detected in peripheral neuropathies, leading to muscle atrophy, such as those related to inflammatory states (32), diabetes (48), or amyotrophic lateral sclerosis (5, 45). Moreover, aging-related sarcopenia and cachexia, as well as genetic-based dystrophies have been reported to be associated with increased in nitrotyrosines levels (2, 18, 41). In rat models of disuse- or denervation-induced atrophy, it has been demonstrated that nNOS detaches from the dystrophin glycoprotein complex associated to the sarcolemmal membrane and redistributes to the cytosol, where it produces NO and activates Forkhead box O (FoxO) transcription factors (61). Although the precise mechanism of NO-mediated FoxO activation is yet to be unraveled, it has been proposed that it could depend on nitration of the inhibitor of NF-κB kinase β (IKKβ) (61). More recently, it has also been demonstrated that nNOS dislocation causes force reduction typical of dystrophin-null (*mdx*) mouse models by means of still not elucidated mechanisms putatively involving tyrosine nitration and also *S*-nitrosylation (34).

S-nitrosylation consists of the covalent, but reversible, addition of an NO moiety to reactive sulfhydryl residues of low- (peptides and aminoacids) and high-molecular-weight molecules (proteins) to generate *S*-nitrosothiol derivatives (SNOs) (15). The *S*-nitrosothiol steady-state level depends on the fine equilibrium between NO production and SNOs reduction. The latter reaction is catalyzed by denitrosylating enzymes, the most important of which is the NADH-dependent *S*-nitrosoglutathione (GSNO) reductase (GSNOR) (9, 21). GSNOR is an evolutionarily conserved and widely expressed enzyme that, by reducing the low-molecular-weight nitrosothiol GSNO, indirectly decreases the concentration of protein SNOs (PSNOs) (35). As previously mentioned, *S*-nitrosylation has been proposed to be involved in muscle alterations typical of neuromuscular disorders (13, 59). In particular, *S*-nitrosylation of protein kinase B (66) and Ryanodine receptor 1 (RyR1) (3, 8, 57) has been observed in aging-related cachexia, during sustained exercise, and in muscle dystrophy. Moreover, NO imbalance and increase in PSNO levels have also been suggested to occur in atrophy-related pathologies, such as cancer and diabetes (28, 61). These alterations, which are frequently associated with mitochondrial fragmentation and dysfunction (52), cause fatigue and myalgia typical of skeletal muscle atrophic states. Interestingly, it has been demonstrated that *N*-acetylcysteine (NAC), a well-known denitrosylating agent, reduces neuropathic pain and ameliorates muscle performance (10, 21, 51), which suggests that *S*-nitrosylation could be deeply implicated in signal transduction underlying neuromuscular homeostasis. Consistent with this, it has been demonstrated that pharmacological inhibition (61) or genetic ablation of nNOS, but not of the inducible form inducible NOS (iNOS) (33, 34), reverts pathological phenotypes. However, these approaches have not enabled discrimination of whether the principal mediator of neuropathy and myopathy induced by NO overproduction was tyrosine nitration or cysteine *S*-nitrosylation.

In this study, by means of a GSNOR-null (GSNOR-KO) mouse model, we have characterized the overall impact of GSNOR deficiency and the resulting *S*-nitrosylation in neuromuscular homeostasis, providing evidence that *S*-nitosylation could represent a common molecular signature of neuropathic and myopathic states.

Results

GSNOR-KO mice show typical features of myopathy

In order to assess whether excessive *S*-nitrosylation could affect muscular function, we performed *S*-nitrosoproteome quantitation by the biotin-switch technique in agreement with Forrester *et al.* (20) that uses ascorbate supplementation in the reduction step without any addition of metals to avoid side effects (*e.g.*, oxygen free radical production) likely affecting sample preparation. It should be mentioned, however, that other publications indicate that this modification is required to enable complete accomplishment of nitrosothiol reduction (63). We verified the reliability of the technique by incubating *tibialis anterior* lysates with or without 2 m*M* of the NO donor DETA NONOate (Supplementary Fig. S1; Supplementary Data are available online at www.liebertpub.com/ars) and next analyzed skeletal muscle tissue from 2-month-old GSNOR-KO and wild-type mice. Figure 1A shows that GSNOR-KO mice had a significant increase in PSNOs levels with regard to their age-matched wild-type counterparts. No change was detected in the expression level of nNOS, iNOS, and endothelial NOS (eNOS) (Fig. 1B). Moreover, no dissociation of nNOS from sarcolemma was detected in GSNOR-KO muscles (Fig. 1C), which is in contrast to distrophin-*null* (*mdx*) mice, selected as they represent a well-documented experimental model of Duchenne muscular dystrophy. In addition, no significant difference was observed in the distribution of iNOS and eNOS between wild-type and GSNOR-KO mice (Supplementary Fig. S2A, B). Finally, no change was detected in the expression levels of thioredoxin 1 (Trx1) (Supplementary Fig. S2C, D), the other major denitrosylating protein besides GSNOR, indicating that the observed PSNOs increase was essentially due to GSNOR deficiency. We then analyzed skeletal muscle morphology and structure using *tibialis anterior* and *gastrocnemius* as elective muscles. Hematoxylin and eosin staining highlighted the presence of a few centro-nucleated myofibers in GSNOR-KO mice and an apparent reduction of

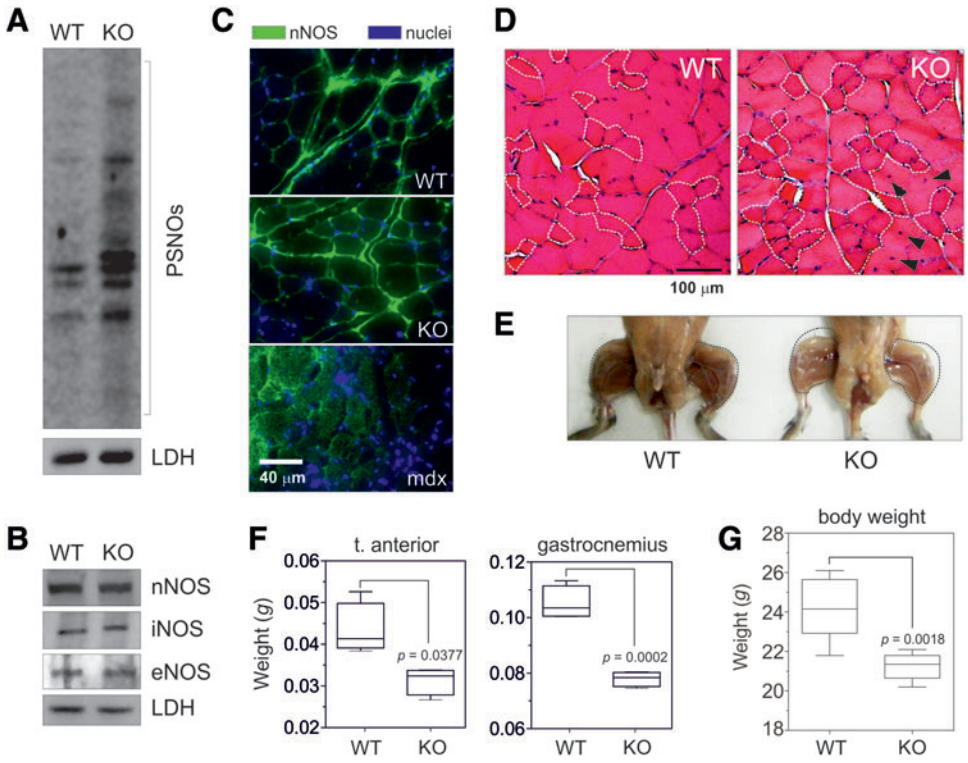

FIG. 1. ***S*-nitrosylation extent and skeletal muscle mass in GSNOR-KO mice. (A)** Evaluation of protein *S*-nitrosothiols (PSNOs) amount in total homogenates of *tibialis anterior* of 2-month-old GSNOR-KO (KO) and wild-type (WT) mice, subjected to biotin-switch assay and revealed by incubation with horseradish peroxidase (HRP)-conjugated streptavidin. Lactate dehydrogenase (LDH) was selected as a loading control from a set of elective ''housekeeping'' proteins on the basis of the coherence between immune-reactive band signal and nitrocellulose Ponceau-Red staining. **(B)** Western blot analyses of neuronal nitric oxide synthase (nNOS), inducible NOS (iNOS), and endothelial NOS (eNOS) performed in *tibialis anterior* homogenates. LDH was selected as a loading control. **(C)** Representative fluorescence microscopy images of *tibialis anterior* sections from KO, WT, and dystrophin-null (*mdx*) mice on staining with anti-nNOS (*green*), and DAPI (*blue*) to highlight nuclei. Scale bar, 40 μm. **(D)** Representative H&E stained sections of *gastrocnemius* of KO and wild-type WT mice. Centro-nucleated myofibers areas including small-sized fibers are indicated (*arrowheads* and white *dotted lines*, respectively). Scale bar, 100 μm. **(E)** Representative picture displaying paws detail of KO and WT mice. *Dotted areas*, muscle volume of WT legs. **(F)** Weight measures of *tibialis anterior* and *gastrocnemius* on tendon-to-tendon isolation from KO and WT mice. Results shown are the means ± SEM of $n = 6$ animals for each group, and the indicated *p*-value was calculated with regard to WT. **(G)** Overall body weight of KO and WT mice. Results shown are the means ± SEM of $n = 6$ animals for each group, and the indicated *p*-value was calculated with regard to WT. To see this illustration in color, the reader is referred to the web version of this article at www.liebertpub.com/ars

myofiber size (Fig. 1D arrowheads and myofibrers surrounded by dotted lines, respectively). This observation was confirmed by in-depth analyses revealing a general decrease in skeletal muscle mass (Fig. 1E, F) that correlated with an overall decrease in body weight (Fig. 1G) and was accompanied by a reduced myofiber cross-sectional area (CSA) (Fig. 2A, B). Since this feature also seemed evident in slow myosin heavy chain (MyHC)-containing type 1 myofibers, we performed parallel analyses in the *soleus*, which contains a high number of these fibers. Figure 2C and D show that CSA of GSNOR-KO *soleus* was similarly reduced (Fig. 2E), indicating that excessive *S*-nitrosylation due to GSNOR deficiency was associated with a general myopathic state.

We then wondered whether these histological features could result in an overall alteration of muscle function. Results obtained by grip tests, shown in Figure 2F, clearly indicate that the muscle strength of GSNOR KO mice was significantly decreased with regard to the wild-type counterpart, both when measured in terms of absolute time that each animal could stay on the grid and when evaluated as the percentage of animals accomplishing the cut-off time (300 s). To confirm these results, we also performed tail suspension tests. When suspended by their tails, wild-type mice tried to maintain their trunk in an extended position and lift it up by spreading out their limbs (37). Conversely, GSNOR-KO mice desisted quite rapidly and retracted their limbs to an adducted position, which has been reported as a behavioral sign of muscle weakness (37). Histograms shown in Figure 2G quantify these observations as the average time passed to the first episode of leg retraction.

GSNOR-KO mice show signs of muscle wasting

On the basis of the obtained results, we performed a real-time PCR analysis of the expression of atrophy-related genes (the so-called ''atrogenes'') in *gastrocnemius* mRNAs from

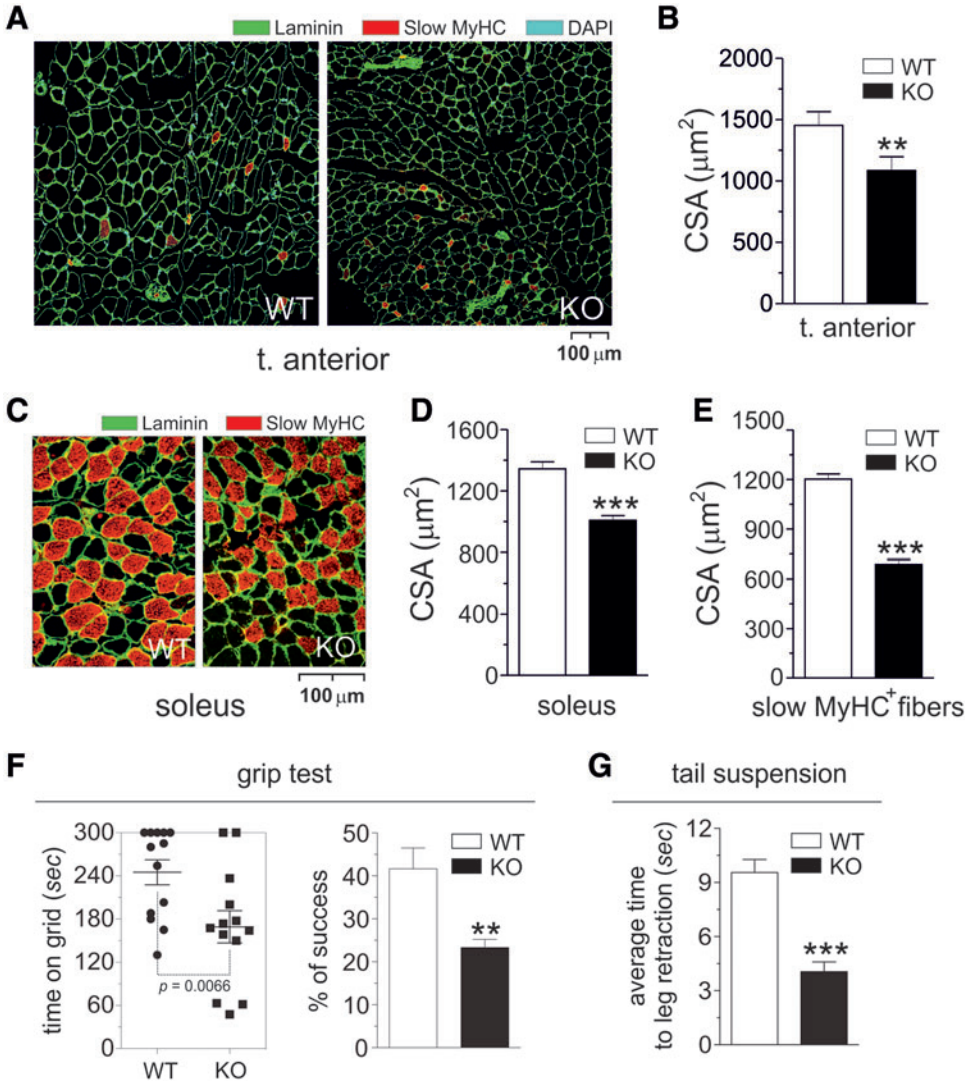

FIG. 2. Size and composition of myofibers of skeletal muscle from GSNOR-KO mice. (A) Representative fluorescence microscopy images of *tibialis anterior* sections from 2-month-old GSNOR-KO (KO) and wild-type (WT) mice on staining with anti-laminin, anti-slow myosin heavy chain (slow MyHC), and DAPI to highlight myofibers boundaries, oxidative fibers, and nuclei, respectively. **(B)** Quantification of fiber cross-sectional area (CSA) in *tibialis anterior* from KO and WT mice. Results shown are the means ± SEM of $n = 6$ animals for each group. $^{**}p < 0.01$ calculated with regard to WT. **(C)** Representative fluorescence microscopy images of *soleus* sections from KO and WT mice on staining with anti-laminin and anti-slow MyHC to highlight myofiber boundaries and oxidative fibers, respectively. Scale bar: 100 μm **(A, C)**. Quantification of total **(D)** and slow MyHC-containing **(E)** fiber cross-sectional area (CSA) in *soleus* from KO and WT mice. Results shown are the means ± SEM of $n = 6$ animals for each group. $^{***}p < 0.001$ calculated with regard to WT. **(F)** Grip test: Evaluation of time that WT and KO mice gripped the grid by both hind and fore legs (*left panel*). Mice that gripped the grip within the cut-off time of 300 s and kept the grip for a further 10 s were recorded as a ''success.'' Percentage of success is reported in the right panel. Results shown are the means ± SEM of $n = 33$ animals divided into three different groups. $^{**}p < 0.01$ calculated with regard to WT. **(G)** Tail suspension test: Average time to the first episode of leg retraction. Results shown are the means ± SEM of $n = 15$ animals divided into three different groups and monitored thrice. $^{***}p < 0.001$ calculated with regard to WT. To see this illustration in color, the reader is referred to the web version of this article at www.liebertpub.com/ars

GSNOR-KO *mdx* mice. Atrogin1 and MuRF1, which are known to be involved in muscle atrophy, were induced in GSNOR-KO conditions. In particular, Atrogin1 mRNA levels were already increased in young individuals, similar to *mdx* mice (Fig. 3A); whereas MuRF1 up-regulation was evident only in the adult mice (Fig. 3B).

In order to evaluate whether the age-dependent increase of atrogenes was related to an increased NOS expression, we performed Western blot analyses of all NOS isoforms in 2- and 12-month-old mice, and compared them with *mdx* samples. Figure 3C shows that nNOS slightly decreased in 12-month-old GSNOR-KO mice, while eNOS protein levels remained constant till adulthood and did not change significantly between wild-type and GSNOR-KO strains. The level of iNOS was also not altered between the two genotypes but underwent a general age-dependent decrease, indicating that

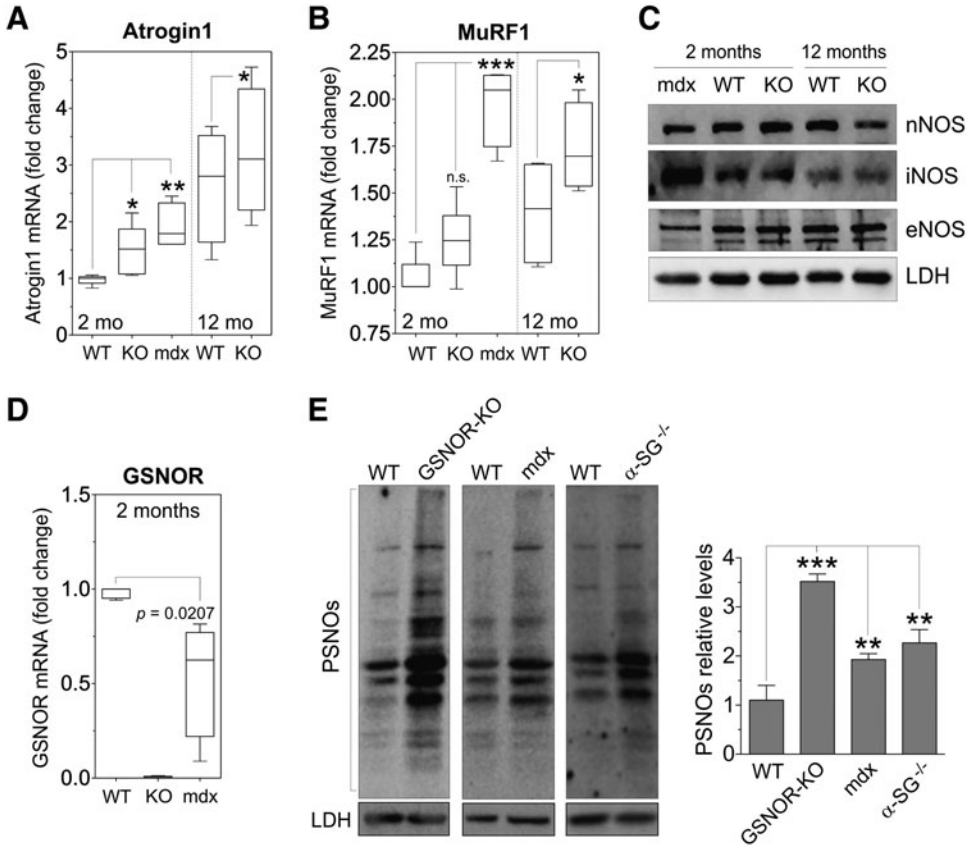

FIG. 3. Atrophy-related gene expression in mouse models of GSNOR deficiency and muscular dystrophies. Quantitative real-time PCR analyses of Atrogin1 **(A)**, MuRF1 **(B)** in *gastrocnemius* of GSNOR-KO (KO) and wild-type (WT) mice at 2 months (2 mo) and 12 months (12 mo) of age. Results shown are the means ± SEM of $n = 12$ animals for each group. $*p < 0.05$; $**p < 0.01$; and $***p < 0.001$ calculated with regard to WT. **(C)** Western blot analyses of nNOS, iNOS, and eNOS performed in *tibialis anterior* homogenates of *mdx*, KO, and WT mice at 2 and 12 months of age. LDH was selected as a loading control. **(D)** Quantitative real-time PCR analyses of GSNOR in *gastrocnemius* of 2-month-old *mdx*, KO, and WT mice. Results shown are the means ± SEM of $n = 4$ animals for each group. *p*-value is calculated with regard to WT **(E)** Evaluation of protein S-nitrosothiols (PSNOs) amount in total homogenates of *tibialis anterior* of 2-month-old KO, *mdx*, α-Sarcoglycan null (α-$SG^{-/-}$), and WT mice, subjected to biotin-switch assay, and revealed by incubation with HRP-conjugated streptavidin. LDH was selected as a loading control. Densitometry of each lane intensity is relativized to LDH and expressed as arbitrary units. Densitometry of immune-reactive bands: Values shown are the means ± SD of $n = 3$ different experiments. $**p < 0.01$; $***p < 0.001$ calculated with regard to WT.

the observed difference in atrogene expressions did not result from an increment in any of the NOS enzymes. Conversely, in line with the recent literature, *mdx* muscles of 2-month-old mice showed a significant increase of iNOS (2), a slight decrease of total nNOS, and no change of eNOS (50) when compared with wild-type muscles. Furthermore, young *mdx* mice exhibited lower levels of GSNOR mRNA (Fig. 3D) and, along with α-Sarcoglycan null (α-$SG^{-/-}$) mice, selected as a further experimental model of muscular dystrophy, showed a significant rise in PSNO levels. This recapitulated GSNOR-KO conditions (Fig. 3E), and indicated that *S*-nitrosylation may represent a common signature of muscle wasting.

GSNOR-KO mice exhibit changes in mitochondrial morphology and autophagy defects

To gain further insights into skeletal muscle tissue alterations induced by *S*-nitrosylation, we performed ultrastructural analyses of *gastrocnemius* by electron microscopy. Figure 4A shows that, with regard to wild-type muscles, the majority of GSNOR-KO myofibers displayed structural alterations of mitochondria, which appeared swollen and were characterized by abnormal cristae morphology (panels b and d *vs.* a and c). Marked alterations in mitochondria inner structure were also evident. Nevertheless, sarcomeres, sarcolemma, and basal lamina appeared normal. The ultrastructural mitochondrial alterations were much more pronounced after physical exercise, with subsarcolemmal mitochondria of GSNOR-KO muscles completely losing their cristae organization (panels f and h *vs.* e and g). However, despite a marked accumulation of such disorganized organelles at the sub-sarcolemmal membrane, GSNOR-KO muscles seemed to show a few mitochondria embedded in double-membraned vacuoles (presumably autophagosomes, arrowheads in panel h). In contrast, the majority of damaged mitochondria present in wild-type muscles were engulfed in autophagosomes, confirming previous data indicating that physical exercise induces autophagy (23, 25). To validate this observation, we performed immunofluorescence analyses of

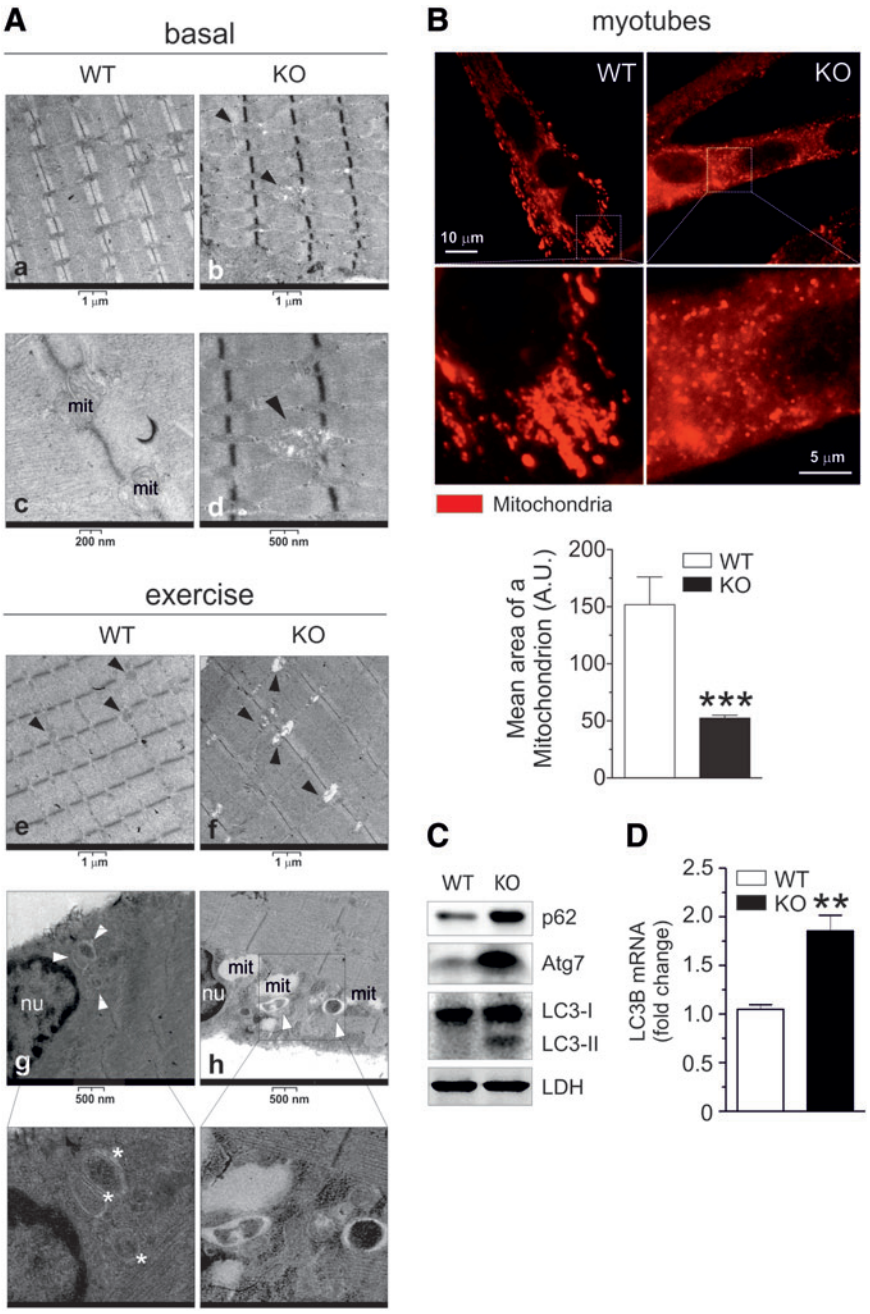

FIG. 4. Mitochondrial morphology and autophagy in skeletal muscle of GSNOR-KO mice. (A) Electron micrographs of gastrocnemius from GSNOR-KO (KO) and wild-type (WT) mice in basal conditions and after physical exercise. Several abnormal mitochondria (*black arrowheads*) are present in myofibers of KO mice in standard condition and after physical exercise (panels *d* and *h*). *Mit*, mitochondria. After treadmill exercise, autophagosomes (*white arrowheads*) are detected in WT and KO mice. Higher magnification images show two *bona fide* autopagosomes (*) **(B)** Representative fluorescence microscopy images of myotubes derived from KO and WT mice on staining with anti-Grp75 to highlight mitochondria. Scale bar, 10 μm and 5 μm for the enlarged view. The quantification of the mean area of a mitochondrion was assessed by *CellProfiler* software. Values shown are the means ± SD of $n = 3$ different experiments. ***$p < 0.001$ calculated with regard to WT. **(C)** Western blot analyses of p62, Atg7, and LC3 (I and II stand for the unlipidated/inactive, and lipidated/active autophagosome-bound form of the protein, respectively) performed in *tibialis anterior* homogenates. LDH was selected as a loading control. **(D)** Quantitative real-time PCR analyses of LC3B performed in *gastrocnemius* KO and WT. Results shown are the means ± SEM of $n = 8$ animals for each group. **$p < 0.01$ calculated with regard to WT. To see this illustration in color, the reader is referred to the web version of this article at www.liebertpub.com/ars

satellite cell-derived myotubes. These results indicated that the mitochondrial network of GSNOR-KO myotubes are fragmented and have lost the typical organization of wild-type cells (Fig. 4B). Such a scenario resembles that previously characterized in collagen VI deficient (*Col6a1*$^{-/-}$) mice, in which an autophagy defect was demonstrated to be the main event underlying the accumulation of abnormal mitochondria (22). In support of autophagy defects in GSNOR-KO muscles, we also observed that the level of p62/sequestosome 1 (p62/SQSTM1 or, simply, p62), which usually undergoes degradation on autophagy induction, was increased (Fig. 4C). However, in contrast with the hypothesis of reduced autophagy, we detected increased levels of autophagy-related gene 7 (Atg7), the master regulator of basal autophagy (46) (Fig. 4C), increased expression of the pro-autophagic microtubule-associated protein 1 light chain 3 (LC3) (Fig. 4D), and the appearance of its lipidated (active) form in the GSNOR-KO background (Fig. 4C). Moreover, when evaluating green fluorescent protein (GFP)-LC3 expressing myotubes from GSNOR-KO mice using fluorescence microscopy, we observed that p62 and LC3 were restricted to discrete spots and up-regulated with regard to the wild-type counterparts (Fig. 5A). In the search for determinants underlying the accumulation of fragmented mitochondria, we measured the ratio between fission and fusion events, by evaluating the expression levels of dynamin related protein 1 (Drp1) and optic atrophy protein 1 (Opa1). As expected, Drp1 was significantly increased; whereas Opa1 was decreased in GSNOR-KO muscles (Fig. 5B), indicating that massive *S*-nitrosylation severely affected mitochondrial dynamics, although it did not seem to result in the induction of selective mitochondrial removal (mitophagy).

It has been demonstrated that mitochondrial fragmentation is the consequence of a decrease in the transmembrane potential

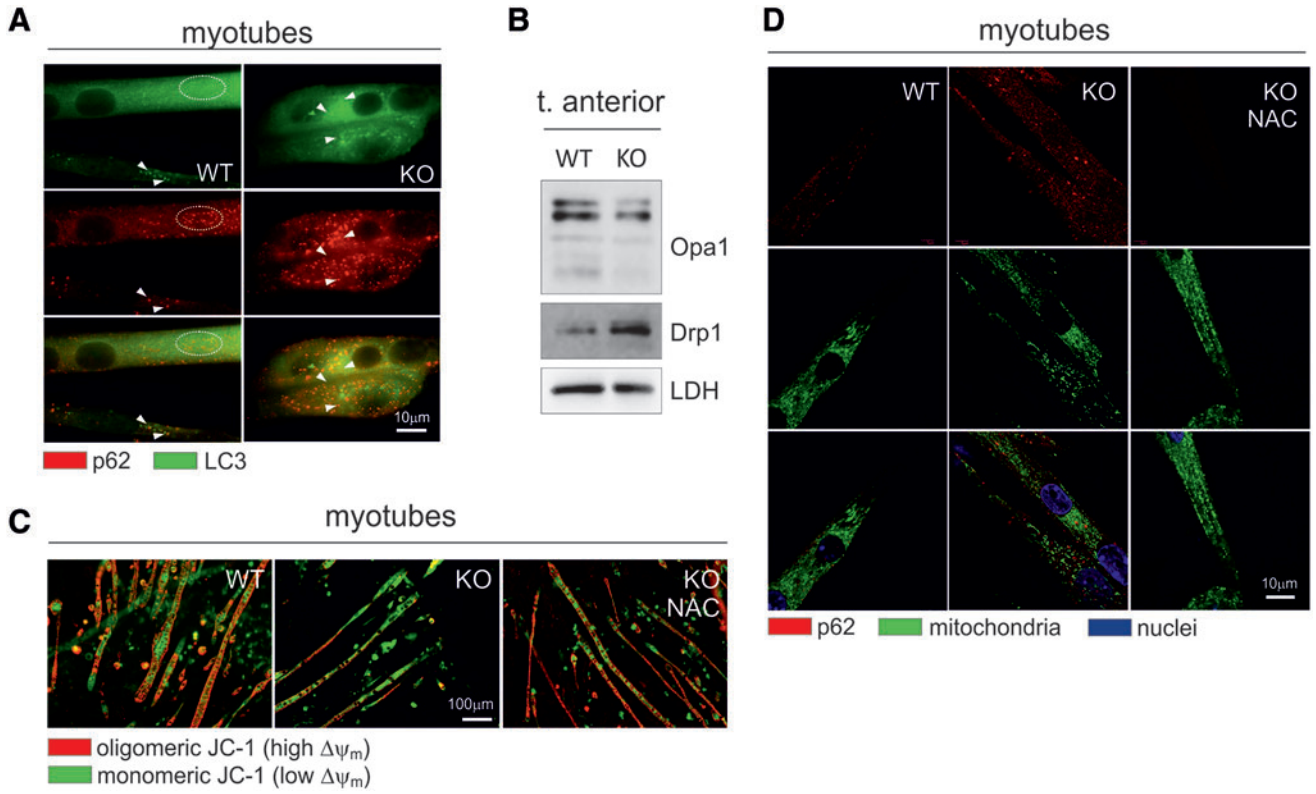

FIG. 5. Mitochondrial autophagy and dynamics in GSNOR-KO models. (A) Representative fluorescence microscopy images of myotubes derived from GSNOR-KO (KO) and wild-type (WT) mice carrying GFP-LC3 in heterozygosis on staining with anti-p62 antibody (*red*). Colocalization between LC3 and p62-positive spots are indicated (*white arrowhead or dotted circle*). Scale bar, 10 μm. **(B)** Western blot analyses of Opa1 and Drp1 performed in *tibialis anterior* homogenates. LDH was selected as a loading control. **(C)** Representative fluorescence microscopy images of myotubes derived from KO and WT mice, incubated or not with 5 m*M* *N*-acetylcysteine (NAC) for 4 h on staining with JC-1. Scale bar, 100 μm. **(D)** Representative fluorescence microscopy images of myotubes derived from KO and WT mice incubated or not with 5 m*M* NAC for 2 h on staining with antibodies anti-p62 (*red*) and anti-Grp75 to visualize mitochondria (*green*), and DAPI for nuclei (*blue*). Scale bar, 10 μm. To see this illustration in color, the reader is referred to the web version of this article at www.liebertpub.com/ars

($\Delta\psi_m$) (42), and that *S*-nitrosylation induces mitochondrial depolarization by compromising the efficiency of respiratory complexes and inducing metabolic hypoxia (15). Therefore, we analyzed $\Delta\psi_m$ of GSNOR-KO myotubes by fluorescence microscopy on staining with the $\Delta\psi_m$-sensitive dye JC-1. The obtained results showed that GSNOR-KO myotubes were depolarized compared with the wild-type genotype, and that treatment with the powerful denitrosylating compound NAC (5 m*M* for 4 h) completely reverted the phenomenon (Fig. 5C). Coherently, NAC treatment restored mitochondrial area and the number of $p62^+$ spots, (Fig. 5D and Supplementary Fig. S3), suggesting that mitochondrial alterations observed on GSNOR deficiency were dependent on *S*-nitrosylation.

Skeletal muscles of GSNOR-KO mice show a mild Nrf2 induction and no sign of tyrosine nitration

Based on the observed increase in PSNOs and alterations in mitochondrial $\Delta\psi$ and morphology, we decided to evaluate whether GSNOR deficiency results in a nitroxidative unbalance, as this has frequently been associated with muscle atrophy (4, 32, 45, 48). Analyses of nitrotyrosine accumulation in sections of *tibialis anterior* (Fig. 6A, B) and a histological examination of lipofuscin (Fig. 6C), which is known to increase on protein nitration (1), indicated that no nitrative stress was present under GSNOR-KO conditions. In fact, nitrotyrosine levels were decreased with regard to the wild-type counterparts. Moreover, we observed a modulation of the cellular antioxidant defense in GSNOR-KO muscles with catalase being the sole antioxidant enzymes induced (Fig. 6D). This is in line with previous results indicating that an increased catalase level is one of the principal markers of muscle wasting induced by denervation and starvation (58). Accordingly, protein carbonyl content only faintly increased (Fig. 6E).

Since these data seemed in conflict with the evident alterations of the mitochondrial network, we asked whether an antioxidant response was constitutively induced in GSNOR-KO systems. Thus, we evaluated whether there was any involvement of Nrf2 and, based on the results so far obtained, we focused on its noncanonical activation induced by the p62-mediated recruitment of Kelch-like ECH-associated protein 1 (Keap1) (31). Western blot analyses of GSNOR-KO and wild-type muscle lysates indicated that, although Nrf2 total levels remained similar, their subcellular amount differed, with the GSNOR-KO muscles showing a mild nuclear accumulation not seen in the wild-type counterparts (Fig. 6F). Similar results were also obtained by immunofluorescence analyses performed

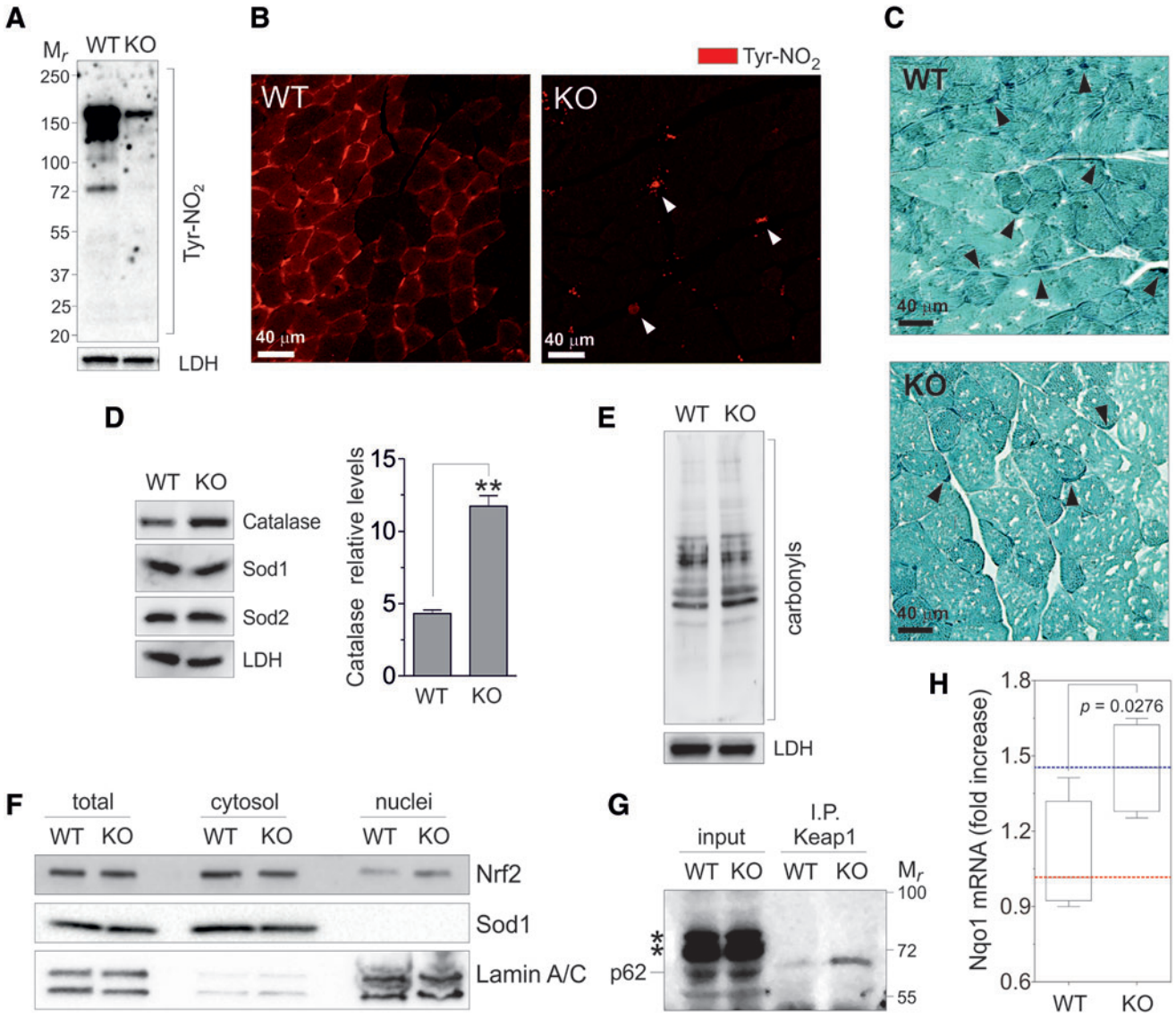

FIG. 6. Nitroxidative status of skeletal muscle of GSNOR-KO mice. (A) Western blot analyses of nitrotyrosines (Tyr-NO_2) performed in *tibialis anterior* homogenates from GSNOR-KO (KO) and wild-type (WT) mice. LDH was selected as a loading control. **(B)** Representative fluorescence microscopy images of *tibialis anterior* sections from KO and WT mice on staining with anti-Tyr-NO_2. Scale bar, 40 μm. *White arrowheads*: blood vessels. **(C)** Representative sections of *tibialis anterior* of KO and WT mice stained with Schmrol ferric-ferricyanide reduction to highlight lipofuscin aggregates. Protein precipitates are indicated (*black arrowheads*). Scale bar, 40 μm. **(D)** Western blot analyses of Catalase, Cu-Zn superoxide dismutase (Sod1), and Mg superoxide dismutase (Sod2) performed in *tibialis anterior* homogenates. LDH was selected as a loading control. Densitometry of immunoreactive bands: Values shown are the means ± SD of $n = 3$ different experiments. $^{**}p < 0.01$ calculated with regard to WT. **(E)** Western blot analyses of protein carbonyls performed in *tibialis anterior* homogenates from WT and KO mice. LDH was selected as a loading control. **(F)** Western blot analyses of Nrf2 performed in total and nuclear and cytosolic enriched fractions of *tibialis anterior* from WT and KO mice. Sod1 and LaminA/C were selected as loading and purity controls of cytosol and nuclei, respectively. **(G)** Immunoprecipitation of Keap1 revealed by Western blot against p62 (*, aspecific bands). **(H)** Quantitative real-time PCR analyses of NADH:quinone oxidoreductase 1 (Nqo1) in *gastrocnemius* of KO and WT mice at 2 months of age. Results shown are the means ± SEM of $n = 6$ animals for each group. *p*-value is calculated with regard to WT. To see this illustration in color, the reader is referred to the web version of this article at www.liebertpub.com/ars

in myotubes of both genotypes (Supplementary Fig. S4A). Moreover, in agreement with our hypothesis, we also observed an increase in the interaction between Keap1 and p62 in *tibialis anterior* of GSNOR-KO mice compared with the wild-type counterparts (Fig. 6G). In line with recent reports (30), we also observed a slight increase in the mRNA level of the Nrf2 downstream gene NAD(P):quinone oxidoreductase 1 (*Nqo1*) (Fig. 6H). In support of these data, we also measured mitochondrial superoxide production by flow cytometry in mouse embryonic fibroblasts (MEFs) and observed a decrease in the GSNOR-KO genotype compared with the wild-type counterpart (Supplementary Fig. S4B).

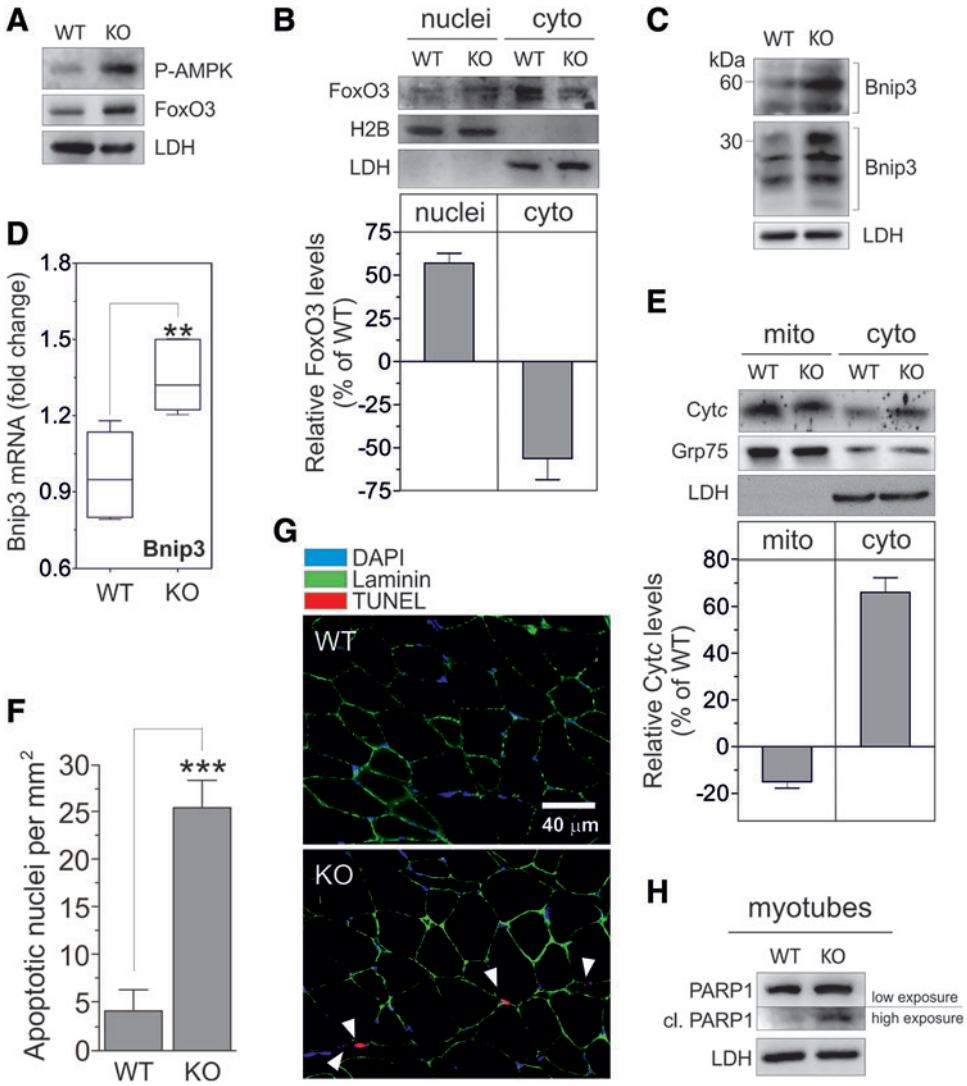

FIG. 7. Phospho-AMPK/FoxO3 pathway and apoptosis in skeletal muscle of GSNOR-KO mice. **(A)** Western blot analyses of phosphorylated AMPK (P-AMPK) and FoxO3 performed in *tibialis anterior* homogenates from GSNOR-KO (KO) and wild-type (WT) mice. LDH was selected as a loading control. **(B)** Western blot analyses of FoxO3 performed in nuclear and cytosolic-enriched fractions of *tibialis anterior*. LDH and histone 2B (H2B) were selected as loading and purity controls. Densitometry of immnoreactive bands: Values shown are the means ± SD of $n = 3$ different experiments relativized to their loading control and calculated as% of WT. **(C)** Western blot analyses of Bnip3 performed in *tibialis anterior* homogenates. LDH was selected as a loading control. **(D)** Quantitative real-time PCR analyses of Bnip3 performed in *gastrocnemius* KO and WT. Results shown are the means ± SEM of $n = 8$ animals for each group. $^{**}p < 0.01$ calculated with regard to WT. **(E)** Western blot analyses of cytochrome *c* (Cyt *c*) performed in mitochondrial and cytosolic-enriched fractions of *tibialis anterior*. LDH and Grp75 were selected as loading and purity controls. Densitometry of immnoreactive bands: values shown are the means ± SD of $n = 3$ different experiments relativized to their loading control and calculated as % of WT. **(F)** Apoptotic (TUNEL$^+$) nuclei calculated in 2-month-old KO and WT mice. Results shown are the means ± SD of $n = 8$ animals for each group. $^{***}p < 0.001$ calculated with regard to WT. **(G)** Representative fluorescence microscopy images of *tibialis anterior* sections from KO and WT mice on TUNEL reaction (to visualize apoptotic nuclei), and staining with anti-laminin and DAPI to highlight myofiber boundaries and nuclei, respectively. *Arrowheads*: apoptotic nuclei. Scale bar, 40 μm. **(H)** Western blot analyses of full-length and cleaved polyADP-ribose polymerase 1 (PARP1) performed in KO and WT myotubes. High exposure has been set up to visualize cleaved immune-reactive bands. LDH was selected as a loading control. To see this illustration in color, the reader is referred to the web version of this article at www.liebertpub.com/ars

AMPK/FoxO3 axis and apoptosis are induced in skeletal muscle of GSNOR-KO mice

Since GSNOR deficiency led to an aberrant mitochondrial phenotype, we wondered whether AMP-dependent protein kinase (AMPK), a well-documented ''energy state-sensing'' protein kinase, could be modulated. Figure 7A shows that AMPK was significantly phosphorylated in GSNOR-KO *tibialis anterior*. This phenomenon correlated with an increase in the total amount of FoxO3 and its nuclear translocation (Fig. 7A, B). These results were in line with Atrogin1 and MuRF1 induction (Fig. 3A, B) and were further substantiated by an

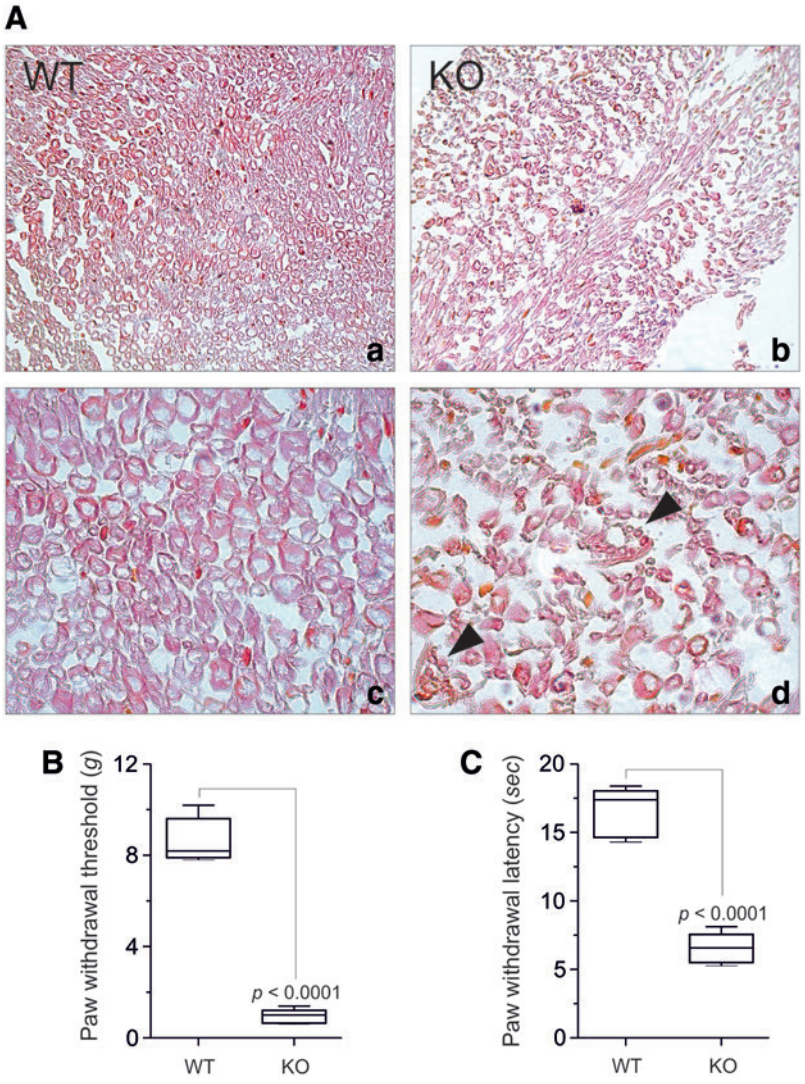

FIG. 8. Axonal damage and neuropathic pain in GSNOR-KO mice. **(A)** Representative Masson's Trichrome stained sections from sciatic nerve of wild-type (WT) **(a, c)** and GSNOR-KO (KO) **(b, d)** mice. **(a, c)** Section of wild-type mice sciatic nerve revealing high number of axons and thick myelin sheath. **(b, d)** Section of KO mice sciatic nerve showing a reduction of axons, regression of myelin, and clustered small myelinated fibers that are indicative of massive regeneration (*arrowheads*). **(c, d)** 2.5-fold magnification of **(a, b)**, respectively Measurement of mechano-allodynia **(B)** and thermal hyperalgesia **(C)** of KO and WT mice. Results shown are the means ± SEM of $n = 10$ animals for each group, and the indicated p-value was calculated with regard to WT. To see this illustration in color, the reader is referred to the web version of this article at www.liebertpub.com/ars

increase of BCL2/adenovirus E1B 19 kDa-interacting protein 3 (Bnip3), a FoxO3-responsive gene promoting mitophagy, detected in GSNOR-KO muscles (Fig. 7C, protein and 7D, mRNA).

We finally evaluated whether GSNOR deficiency-induced mitochondrial fragmentation could result in the induction of apoptosis and, in turn, contribute to muscle wasting. To this aim, we analyzed cytochrome *c* distribution, and found that, in this background, it was released from mitochondria into the cytosol (Fig. 7E). Moreover, TUNEL assay indicated that GSNOR-KO *tibialis anterior* showed a significant increase in apoptotic nuclei (Fig. 7F, G). These results, along with the evidence that polyADP-ribose polymerase 1 (PARP1) cleavage occurred in GSNOR-KO myotubes (Fig. 7H), suggested that GSNOR-KO muscular models were primed to undergo apoptosis.

GSNOR-KO mice show clear signs of neuropathy and delay of muscle regeneration

Denervation or peripheral nerve injuries, such as those associated with a partial loss of fibers or myelin in the nerve, can strongly contribute to muscle wasting (29). Therefore, to assess whether GSNOR deficiency could indirectly induce muscle atrophy also by affecting the nerve healthy state, we performed histological analyses of sciatic nerve from both GSNOR-KO and wild-type mice. Changes in the architecture of the nerves were clearly evident, as we observed significant axonal damage, as well as a reduction of the myelin sheath, that varied in thickness (Fig. 8A panel b and d *vs.* a and c). A high number of clustered small myelinated fibers was also evident as a marker predictable of massive regeneration (Fig. 8A panel d, arrowheads). Since these features supported the hypothesis that GSNOR deficiency was associated with neuropathy, we evaluated the response to nociceptive stimuli. Measurement of neuropathic pain in terms of both mechano-allodynia (Fig. 8B) and thermal hyperalgesia (Fig. 8C) revealed that 2-month-old GSNOR-KO mice dramatically developed peripheral neuropathic pain when compared with age-matched wild-type mice.

On the basis of these results indicating that peripheral nerves were severely compromised in the GSNOR-KO background, we evaluated the capability of GSNOR-KO muscles to regenerate. Indeed, it is well known that muscle fibers which fail to become re-innervated, or that are unable

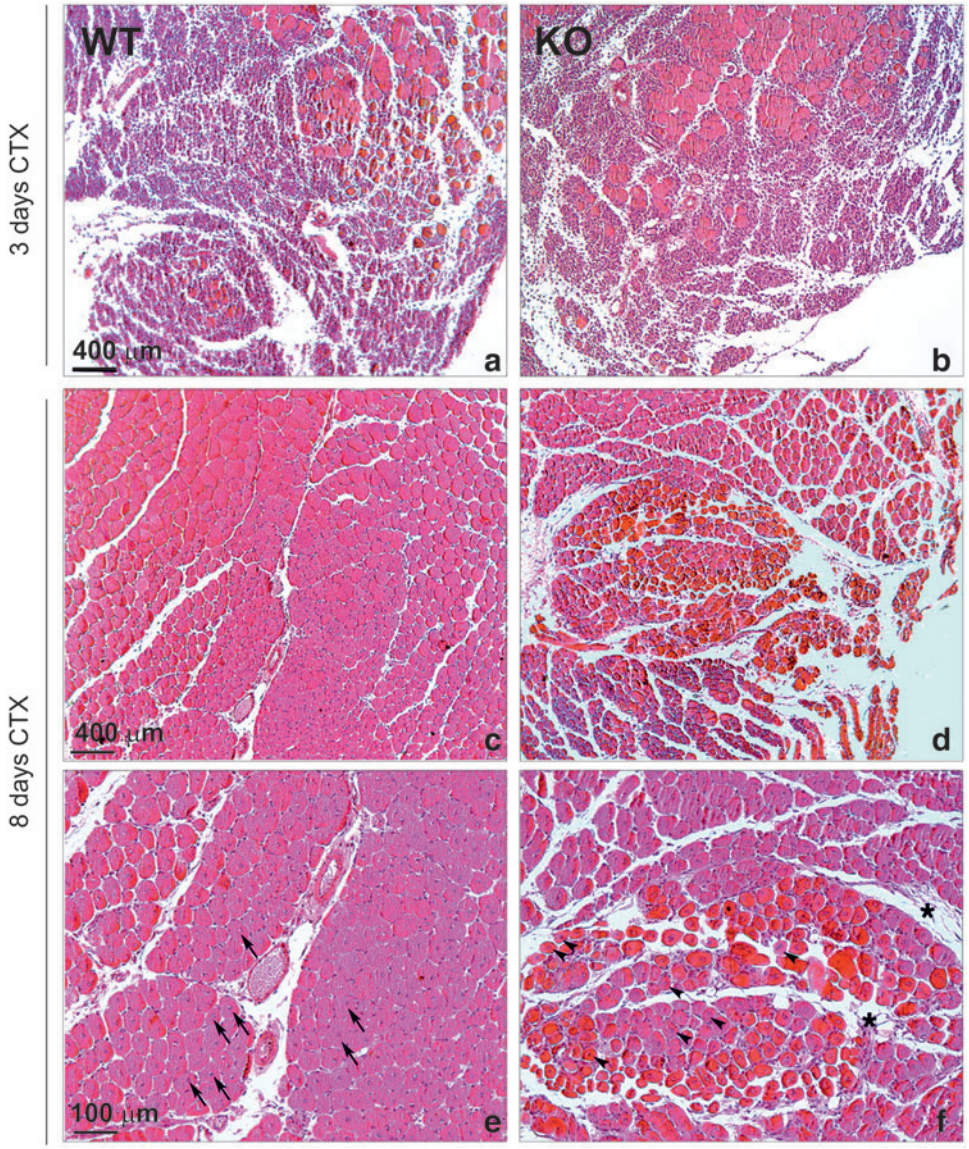

FIG. 9. Delay of muscle regeneration in GSNOR-KO mice. Representative H&E stained sections from *tibialis anterior* of wild-type (WT) **(a, c, e)** and GSNOR-KO (KO) **(b, d, f)** mice at 3 **(a, b)** and 8 **(c–f)** days after cardiotoxin (*CTX*) injection-induced injury. **(a, b)** Acute muscle damage revealing massive inflammatory infiltration and degenerating muscles in WT as well as in KO mice. **(c)** Semi-complete regeneration process at a later stage in wild-type mice. **(e)** Enlarged view of **(c)** showing a few regenerating centro-nucleated myofibers with dimensions comparable with undamaged fibers (*arrows*). **(d)** Damaged *tibialis anterior* of KO mice, showing a remarkable delay in the regenerative capability. **(f)** Enlarged view of **(d)** presenting a large portion of small centro-nucleated muscle fibers (*arrowhead*) surrounded by abundant extracellular matrix accompanied still by a few inflammatory cells (*asterisk*). Scale bar: 400 μm **(a–d)** and 100 μm **(e, f)**. To see this illustration in color, the reader is referred to the web version of this article at www.liebertpub.com/ars

to respond to re-innervation, undergo progressive atrophy (49). We injected cardiotoxin (CTX) into *tibialis anterior* of GSNOR-KO and wild-type mice to evoke acute muscle damage and then assessed the ability of muscles to regenerate. Histological analyses of *tibialis anterior* from GSNOR-KO and wild-type mice at 3 days after CTX injection revealed acute muscle damage that resulted in degeneration of myofibers accompanied by massive inflammatory infiltration in both phenotypes (Fig. 9, panels a and b). Eight days after CTX treatment, wild-type mice showed an almost complete regeneration process, with muscles still presenting several centro-nucleated muscle fibers (arrows in Fig. 9, panel e) of comparable size to undamaged fibers (Fig. 9, panels c and e). Conversely, GSNOR-KO mice displayed very small regenerating centro-nucleated myofibers (Fig. 9, arrowheads in panel f) that were still surrounded by abundant extracellular matrix and a few inflammatory cells (Fig. 9, panels d and f), revealing a marked delay of the muscle regeneration process in the GSNOR-KO mice.

Discussion

The role of nNOS dislocation from the sarcolemma and the subsequent cytosolic production of NO have been associated with neuromuscular dysfunctions (61, 65). Moreover, NO has been proposed to play an active role in the loss of muscle fibers and in the development of peripheral neuropathy associated with different pathological states (27, 32), such as aging-related sarcopenia (24), diabetes (43, 48), cancer and chemotherapy, and neurological disorders (45, 62). In particular, NO has been implicated in the activation of FoxO3a-dependent degradation of muscle proteins (61), and in the hyperactivation of RyR1, which leads to Ca^{2+} leakage (57, 60), mitochondrial fragmentation (42) and, ultimately, results in muscle atrophy. Interestingly, NO overproduction has also very recently been documented to be associated with transduction pathways underlying neuropathic pain perception resulting from muscle wasting (12). Nevertheless, despite the large number of observations regarding the deleterious role of

NO in neuromuscular disorders, it is still unclear whether nitroxidative damage is the principal causative event of the pathological phenotype, or whether this depends on the activation of cysteine *S*-nitrosylation-based signals. Moreover, no evidence about the possible impact of denitrosylation reactions (*e.g.*, those mediated by GSNOR) on neuromuscular disorders has been provided so far. In this work, we focused on these aspects and demonstrated that GSNOR deficiency induces a significant increase of PSNOs in skeletal muscle tissue and results in a clinically relevant neuromuscular phenotype with evident signs of myopathy and neuropathy. A proteomic analysis of the muscle proteome should be done in the future in order to gain a detailed understanding of which proteins undergo *S*-nitrosylation, and how this modification can impact their function/expression.

GSNOR-KO mice suffer from sarcopenia and muscle wasting without any apparent involvement of tyrosine nitration-associated damage. Our results indicate that bulk autophagy induction, atrogene expression, and apoptosis are active processes associated with muscle loss, even though GSNOR-KO conditions are not as pathologically evident as observed in well-recognized mouse models of muscle dystrophies, namely *mdx* and α-$SG^{-/-}$ mice. The muscular phenotype observed in GSNOR mutant mice argues for *S*-nitrosylation being associated with an early aging process, and, therefore, this phenotype may better resemble an aging-related sarcopenia or cachexia, rather than atrophy. This hypothesis is strengthened by the observed delay in muscle regeneration and by the evidence that GSNOR deficiency affects nerve myelination and axon integrity, and dramatically results in neuropathic pain: conditions which are associated with muscle wasting in elderly people. Interestingly, it has been reported that GSNOR KO mice show an increase in the incidence of hepatocellular carcinoma (HCC), which can be diagnosed at 18 months of age (64). Although myopathic and neuropathic states can be comprised within the canonical clinical picture of cancer, it should be taken into consideration that our study has mostly been performed in 2 month-old mice, an age at which no animals shows any symptoms, or has been reported to develop HCC. Therefore, it can be assumed that the neuromuscular phenotype is an early pathological condition compared with cancer onset and, most likely, not related to the propensity to develop HCC due to GSNOR deficiency.

It has recently been shown that peroxynitrite resulting from NO overproduction and NADPH oxidase activation is implicated in central sensitization which is responsible for mechanoallodynia and thermal hyperalgesia. Although the precise mechanisms are not yet fully understood, putative nitration of Sod2, glutamine sinthetase, and L-glutamate transporter 1, involved in the pathways of free radical production and glutamate turnover, respectively (17), were suggested to be the causative events underlying pain development. In this work, we propose that protein *S*-nitrosylation is also critical in the pain pathway and could represent an additional (reversible) post-translational modification implicated in the central sensitization leading to pain sensibility. We cannot establish whether myopathy derives from neuropathic states or *vice versa*, or whether both contribute to the pathological phenotype. Work is in progress in our laboratory to understand this issue and its marked impact on muscle physiology. With regard to this aspect, grip strength and tail suspension tests performed provide the first evidence that young GSNOR-KO mice show clear signs of muscle weakness, further supporting the idea that *S*-nitrosylation could be implicated in both neuropathic pain and muscle dysfunction. This feature also correlates with the evident mitochondrial alterations observed in GSNOR-deficient systems. It is now accepted that *S*-nitrosylation affects mitochondrial respiratory complexes (15, 47) and that this induces metabolic hypoxia, resulting in ATP decrease and mitochondrial depolarization (40), a preparatory condition for mitochondrial fragmentation (11). Accordingly, we observed a significant decrease of mitocondrial $\Delta\psi$ along with an increase of the phospho-active form of AMPK, which resulted in an aberrant accumulation of fragmented mitochondria, both *in vivo* and *in vitro*, suggesting that mitochondria are impaired, although not properly and selectively removed by mitophagy in GSNOR mutant conditions. Nevertheless, in contrast to other types of well-documented atrophic states in which bulk autophagy is inhibited [*e.g.*, *Col6a1* mutation-dependent Bethlem and Ullrich muscular dystrophies (22)], our data argue that this process is activated in the GSNOR-KO mice. This apparent paradox, which is already under investigation in our laboratory, is reinforced by the observation that Bnip3, a FoxO3 target gene involved in mitochondrial removal by autophagy, is induced in GSNOR-KO conditions, confirming that FoxO3-dependent transcription is activated in our system.

Although apparently conflicting with a recent study reporting that NO inhibits the early steps of bulk autophagy (53), our results should be considered a complement to that, as they are obtained using different experimental conditions. Indeed, Sarkar *et al.* make use of NO donors or take advantage of NOS up-regulation to induce nitrosative stress. Moreover, they point out that the increase in Bcl2/Beclin1 interaction, which should contribute to autophagy inhibition, is completely unrelated to Bcl2 *S*-nitrosylation (53). Differently, in our study we have selected a genetic model of *S*-nitrosylation, without affecting NO fluxes. In fact, we have demonstrated that no modulation of the expression and distribution of NOS isoforms occurs in GSNOR-deficient mice. By considering all this evidence, we propose that NO imbalance generally affects autophagy. In particular, its overproduction inhibits bulk autophagy through various processes, including *S*-nitrosylation; whereas modulating *S*-nitrosylation only seems to selectively compromise mitophagy.

The pivotal role of *S*-nitrosylation in mitochondrial fragmentation and depolarization has been confirmed by NAC treatment that rescues both mitochondrial network and $\Delta\psi_m$. Although NAC can also function as an ROS-scavenging compound, contributing to *de novo* synthesis of glutathione, the evidence that GSNOR-KO systems show a decrease in mitochondrial superoxide production enables us to speculate that NAC, in fact, acts as a denitrosylating more than an antioxidant molecule. The hypothesis that ROS do not play any detrimental role in GSNOR-KO models is also corroborated by the constitutively basal induction of the antioxidant response-inducing factor Nrf2. In particular, we found out that in GSNOR KO muscular models, p62 interacts with Keap1, and Nrf2 accumulates into the nuclei even in basal conditions. This event (i) induces a mild transcription of *Nqo1*, which contributes toward decreasing the production of mitochondrial superoxide; (ii) provides a rationale for nitrotyrosine decrease, arising from the encountering between NO and superoxide; (iii) justifies the high levels of p62 as a non-canonical activator of Nrf2 (30, 31); and (iv) represents one likely mechanism for adaptation to conditions of

nitrosative stress. Moreover, this finding is perfectly in line with a very recent publication in which it has been observed that GSNOR-KO livers show a basal increase of nuclear Nrf2, which becomes much more pronounced on exogenous insults (namely, paracetamol intoxication) (14).

Materials and Methods

Animals and treatments

All mouse experiments were conducted in accordance with the European Community guidelines and with the approval of relevant National (Ministry of Health) and local (Institutional Animal Care and Use, Tor Vergata University) ethical committees. The GSNOR KO mouse strain, generated on a C57BL/6 genetic background, was originally provided by Professor Jonathan S. Stamler (Institute for Transformative Molecular Medicine, Case Western, Cleveland) (36), while the C57BL/6 wild-type mice strain was purchased from Charles River. Dystrophin mutated *mdx* and α-sarcoglycan null (α-$SG^{-/-}$) mice were from Jackson Laboratories. To generate GSNOR-KO GFP-LC3 heterozygous mice, we crossed GSNOR-KO C57BL/6 mice with GFP-LC3 homozygous transgenic mice (Ref. 39, kindly provided by Prof. Mizushima, Department of Physiology and Cell Biology, Tokyo Medical and Dental University, Tokyo, Japan to Francesco Cecconi). F1 mice were backcrossed with each other, and the resulting F2 population was genotyped in order to select GSNOR-KO mice that were homozygous for GFP-LC3. These mice were then crossed with mice of the GSNOR-KO genotype to obtain strains that were heterozygous for GFP-LC3. This model enables a correct evaluation of differences in the rate of autophagy. Mice were housed in an environmentally controlled room (23°C, 12 h light-dark cycle) and provided with food and water ad libitum.

Muscle injury/regeneration. Muscle injury was conducted in 2-month-old mice, by injecting 30 μl of 10 μM cardiotoxin (Latoxan) in *tibialis anterior*. Muscles were then harvested at different time points after injury, with uninjected contralateral *tibialis anterior* muscles as a control.

Exercise. Treadmill exercise was carried out by subjecting mice to forced run in a treadmill device. Briefly, mice were first left to adapt to the treadmill for 5 min at a speed of 5 cm/s. Then, exercise was performed by starting at a speed of 10 cm/s that was increased with 2 cm/s every 2 min until a maximum of 40 cm/s. Mice were left running until exhaustion. The experiment was repeated for 5 days. Mice were sacrificed by cervical dislocation, and muscles were dissected.

Behavioral testings

Mechano-allodynia. Mechanical withdrawal thresholds were taken using calibrated von Frey filaments (Stoelting Co.) ranging from 3.61 (0.407 *g*) to 5.46 (26 *g*) bending force, according to the ''up-and-down'' method (16). Mice were examined on 15 min of adaptation; after that, the development of mechano-allodynia was measured as the reduction in mechanical mean absolute paw withdrawal thresholds (*g*) at forces which failed to elicit withdrawal responses (baseline).

Thermal hyperalgesia. Hyperalgesic responses were determined by the Hargreaves method using a Basile plantar test (Ugo Basile) that was set up on 30 IR with a cutoff latency of 20 s employed to prevent tissue damage. Mice were individually confined to Plexiglas chambers and allowed to adapt for 15 min before behavioral testing. A mobile infrared generator was positioned to deliver a thermal stimulus directly to an individual hind paw from beneath the chamber. The withdrawal latency period was determined with an electronic clock circuit and thermocouple. Two readings were acquired for each paw to determine a mean latency for each animal. Thermal hyperalgesia is expressed as the mean latency for each group and expressed as paw withdrawal latency (sec).

Grip test. Grip strength was evaluated by placing the animals onto a horizontal grid, and measuring the time until they fell down; the cut off time was 300 s. If the mice gripped the grid by both hind and fore legs within the cut-off time of 300 s and kept the grip for a further 10 s, they were recorded as being a ''success.'' Three different groups were analyzed with each group containing approximately 13 mice, all of which were analyzed twice on 2 different days, each time in three repetitions with 30-min intervals.

Tail suspension. Each animal was suspended in mid-air by the tail for a period of 12 s, and the time passed to the first episode of leg retraction was recorded; this procedure was repeated thrice, and the average time passed to the first episode of retraction for each mouse was calculated.

Transmission electron microscopy

Gastrocnemius muscles were fixed with 2.5% glutaraldehyde (Sigma) in phosphate buffer 0.1 *M* (pH 7.4) and embedded in Epon E812 resin (Sigma). Ultrathin sections were stained with uranyl acetate (Sigma) and lead citrate (Sigma), and they were observed in a Tecnai-G2 F12 (FEI) electron microscope.

Histology and tissue immunofluorescence

On cervical dislocation, *tibialis anterior*, *gastrocnemius* or *soleus* muscles, and sciatic nerve were dissected and fixed in 4% paraformaldehyde/PBS (pH 7.4) for 5 h at 4°C; infiltrated sequentially with 10%, 20%, and 30% sucrose (Sigma); embedded in O.C.T. compound (Bio-Optica); and flash frozen in liquid nitrogen-cooled isopentane (VWR Interantional). Sections were cut to a thickness of 8 μm using a Leika cryostat and used for immunostaining or histological staining.

Histology. Serial muscle sections were obtained and stained in H&E and Masson's Trichrome following standard procedures. Lipofuscin staining was performed by the Schmrol ferric-ferricyanide reduction test as previously described (1).

Immunofluorescence. Cryosections of *tibialis anterior* or *soleus* were fixed in 4% paraformaldehyde in PBS for 10 min at 4°C and washed in PBS. After permeabilization with 0.2% Triton X-100 (Sigma) and 1% BSA (Sigma) in PBS for 30 min, the samples were blocked in 10% horse serum (Sigma) in PBS at room temperature and then incubated for 1 h with primary antibodies. The following primary antibodies were

used: anti-laminin (Sigma; 1:500); anti-slow MyHC (Sigma; 1:1000); anti-nitrotyrosine (Life-Technologies; 1:100); and anti-nNOS, iNOS, and eNOS (Santa Cruz; 1:100). Cryosections were then washed in blocking buffer and incubated for 1 h with labeled secondary antibodies (Life-Technologies).

Apoptotic nuclei were visualized by TUNEL fluorescent assay (Roche Diagnostic). Nuclei were visualized with the DNA dye Hoechst (Life-Technologies) and examined under a Leica TCS SP5 confocal microscope. Fluorescence images were adjusted for brightness, contrast, and color balance using Adobe Photoshop CS.

Morphometric analysis

Myofiber CSA was assessed on *tibialis anterior* and *soleus* cryosections by using ImageJ software (http://rsb.info.nih.gov/ij/) (NIH). Three laminin/slow-MyHC stained cross-sections from three different mice for each genotype were analyzed. Between 100 and 300 fibers were counted. Values shown are the average of CSA of all wild-type and GSNOR-KO *tibialis anterior* or *soleus* fibers. In the *soleus*, the same fibers considered for CSA were also counted for positive slow-MyHC labeling. CSA values of *tibialis anterior* and *soleus* were calculated and expressed in μm^2.

Satellite cell isolation and myotube culture and treatment

Single muscle fibers with associated satellite cells were isolated as described (44). Briefly, the hind limb muscles were digested with collagenase; single myofibers were cultured in GM1 [DMEM supplemented with 10% horse serum (Lonza), supplemented with 0.5% chick embryo extract (MP biomedicals), penicillin-streptomycin (Lonza)] at 37°C in suspension for 72 h, and then plated on matrigel (Sigma; 1 mg/ml ECM gel)-coated dishes for satellite cell culture. After 3 days, the fibers were removed and the medium was replaced with proliferation medium (GM2: 20% FBS, 10% horse serum, and 1% chick embryo extract in DMEM).

After 5 days of proliferation, satellite cells were allowed to differentiate into myotubes by replacing the growth medium with differentiation medium (DM: 2% HS and 0.5% chick embryo extract in DMEM). Four days after differentation, NAC (Sigma; final concentration 5 m*M*) was added for 2 and 4 h.

JC-1 (Life technologies) was added to prewarmed cell medium at a final concentration of 5 μg/mL in order to evaluate $\Delta\psi_m$. After incubation for 10 min at 37°C, cells were washed in PBS and analyzed using an EVOS Floid Cell Imaging Station (Life Technologies).

Myotube fluorescence analyses

Myotubes grown on cover slips were washed twice with cold PBS and fixed in 4% paraformaldehyde in PBS for 10 min at room temperature. Cells were washed twice with cold PBS and incubated for 45 min with anti-Grp75 (Stressgen; 1:1000), or anti-p62/SQSTM1 (MBL; 1:500), or anti-NRF2 (Santa Cruz; 1;100) antibodies diluted in cold blocking buffer (PBS supplemented with 10% FBS). Cells were then washed with cold PBS and incubated for an additional 30 min with appropriate fluorophore-conjugated secondary antibodies (AlexaFluor 488 and 568; Life-Technologies). After incubation, cells were washed with PBS, and nuclei were stained with 10 μM Hoechst for 10 min, before an additional wash in PBS and mounting on observation slides. Images were captured by using a Delta Vision (Applied Precision) Olympus 1×70 microscope.

Mitochondrial area was assessed by *CellProfiler* software on at least 60 mitochondria. Mitochondria were selected manually, and their average area was expressed in a graph as arbitrary units (A.U.). Similarly, p62-positive spots were quantified by *CellProfiler* software in terms of number/myotube and average area and expressed as arbitrary units (A.U.).

To evaluate mitochondrial integrity, cells were stained with 50 n*M* of the $\Delta\psi_m$-sensitive fluorescent probe Mitotracker Red (Molecular Probes, Life Technologies), washed, and analyzed cytofluorometrically

MEFs isolation and culture

MEFs primary cells were prepared from embryos at E13.5, cultured in DMEM supplemented with 10% FBS, and utilized for experiments from the second to the fourth passage in culture.

Mitochondrial superoxide evaluation and analysis

MEFs were incubated with 5 μM MitoSOX (Life Technologies) for 10 min at 37°C. Cells were then washed, trypsinized, resuspended in ice-cold PBS, and collected.

The fluorescence intensities were monitored by an FACScalibur instrument (Becton Dickinson)

Western blotting

Tissue samples from *tibialis anterior* were homogenized in a lysis buffer containing 50 m*M* Tris-HCl (pH 8.0), 150 m*M* NaCl, 1% NP-40, and 12 m*M* Na-deoxycholate (Sigma) that was supplemented with protease and phosphatase inhibitors cocktail (Merck). Nuclei and mitochondria were obtained as previously described (19). Lysates were centrifuged at 13,000 rpm for 10 min at 4°C to discard cellular debris. Protein concentration was determined by the Lowry protein assay (Bio-Rad Laboratories). Proteins were separated by SDS-PAGE and transferred to nitrocellulose membranes (GE Healthcare Life Science Europe) that were probed with the following antibodies: anti-nNOS (Santa Cruz), anti-iNOS (Santa Cruz), anti-eNOS (Santa Cruz), anti-Opa1 (BD Biosciences Buccinasco), anti-Drp1 (BD Biosciences), anti-p62 (MBL), anti-phospho-AMPKα-Thr172 (Cell Signaling), anti-cytochrome c (Santa cruz), anti-Sod1 (Santa Cruz), anti-Sod2 (Merck), anti-catalase (Sigma), anti-Bnip3 (Sigma), anti-nitrotyrosine (Cayman), anti-LC3 (Sigma), anti-FoxO3 (Santa Cruz), anti-Trx1 (Cell Signaling), anti-lactate dehydrogenase (LDH) (Santa Cruz), anti-PARP1, and anti-actin (Santa Cruz). After immunostaining with appropriate secondary horseradish peroxidase-conjugated goat anti-rabbit or anti-mouse antibodies (Sigma), bands were revealed by a Fluorchem Imaging system (Alpha Innotech), using the Amersham ECL detection system (GE Healthcare Life Science) and quantified by densitometry. Carbonylated proteins were detected using the Oxyblot Kit (Intergen) after a reaction with 2,4 dinitrophenylhydrazine (DNP) for 15 min at 25°C. Samples were then resolved by 10% SDS polyacrylamide gel electrophoresis, and DNP-derivatized proteins were identified by immunoblot using an anti-DNP antibody (19).

Table 1. Primers Used in Real-Time Polymerase Chain Reaction

Gene	*Forward primer*	*Reverse primer*
HPRT	5′-GCAGTACAGCCCCAAAATGG-3′	5′-GGTCCTTTTCACCAGCAAGCT-3′
Atrogin1	5′-GCGACCTTCCCCAACGCCTG-3′	5′-GGCGACCGGGACAAGAGTGG-3′
MuRF1	5′-AGGGGCTACCTTCCTCTCAAGTGC-3′	5′-TCTTCCCCAGCTGGCAGCCC-3′
GSNOR	5′-TCACTTCATGGGGACTAGCA-3′	5′-CCGAGGGATCGATTTTAGCA-3′
LC3B	5′-CGTCGCCGGAGTCAGATCGTC-3′	5′-CCACTCTTTGTTCAAAGCTCCGGC-3′
p62	5′-TGTGGAACATGGAGGGAAGAG-3′	5′-TGTGCCTGTGCTGGAACTTTC-3′
Bnip3	5′-GAAGCGCACAGCTACTCTCA-3′	5′-TCCAATGTAGATCCCCAAGCC-3′
Nqo1	5′-CGCCTGAGCCCAGATATTGT-3′	5′-GCACTCTCTCAAACCAGCCT-3′
Trx1	5′-ATGTGGATGACTGCCAGGATG-3′	5′-CCTTGTTAGCACCGGAGAAC-3′

Selection of loading control. LDH was selected as a loading control, as GADPH protein levels changed significantly between WT and KO muscles, even though total protein amounts were comparable. Actin and tubulin levels also differed markedly in spite of the equal protein content loaded, as their levels and stability are known to be modulated by *S*-nitrosylation. Quantitative real-time PCR analyses of *Ldh* mRNA, along with the mRNA of the housekeeping gene (internal control) *Hprt* (hypoxanthine-guanine phosphoribosyltransferase) normalized to 18S rRNA, confirmed that there was no modulation of LDH expression in GSNOR-KO conditions (data not shown).

PSNOs

S-nitrosylation assays were performed as previously described (20). For the biotin-switch assay, muscles were homogenized in HEN buffer (25 m*M* HEPES, 50 m*M* NaCl, 0.1 m*M* EDTA1% NP-40, protease inhibitors, pH 7.4). Free cysteine residues were blocked with *S*-methyl methanethiosulfonate (MMTS; Sigma). More specifically, 0.5–2 mg of protein samples were diluted to 1.8 ml with HEN buffer (100 m*M* HEPES, 1 m*M* EDTA, 0.1 m*M* neocuproine, pH 8.0). Next, 0.2 ml of 25% SDS was added along with 20 μl of 10% MMTS (to reach a final volume of 2 ml and final concentrations of 2.5% SDS and 0.1% MMTS), and incubated at 50°C in the dark for 15–20 min with frequent vortexing. Three volumes of cold acetone were added to each sample. Proteins were precipitated for 20 min at −20°C, and collected by centrifugation at 2000 *g* for 5 min. Supernatant was discarded, and protein pellets were gently washed with 70% acetone at 4°C. Proteins were resuspended in 0.24 ml HENS buffer (HEN buffer with 1% SDS) and transferred to a fresh 1.7 ml microfuge tube containing 30 μl biotin-HPDP (2.5 mg/ml) with or without sodium ascorbate (20 m*M*). After incubation with the horseradish peroxidase-conjugated streptavidn (Merck), biotinylated proteins were revealed using the Amersham ECL detection system (GE Healthcare Life Science). Ascorbate-free samples have been omitted for straightforward visualization and interpretation of data. Reliability of the technique has been further tested by incubating *tibialis anterior* lysates with or without 2 m*M* of the NO donor DETA NONOate for 30 min at room temperature in order to artificially induce *S*-nitrosylation of muscle proteins (Supplementary Fig. S4).

Immunoprecipitation assays

Immunoprecipitations were performed by adding 1 μg of anti-Keap1 antibody (Santa Cruz) to 50 μl of prewashed Dynabeads®-protein G (Invitrogen) to whole tissue extracts from skeletal muscle.

For each reaction, 500 μg of total protein were incubated with Dynabeads-Ab complex. After 1 h at room temperature, beads were recovered and washed six times with RIPA buffer. Immunoprecipitated proteins were detached from beads by boiling in sample buffer, separated by SDS-PAGE, transferred to nitrocellulose membranes (Amersham Pharmacia), and then incubated with anti-p62 antibody (MBL).

Real-time PCR

Tissue samples were homogenized in TRI Reagent (Sigma), and RNA was extracted in accordance with the manufacturer's protocol. Total RNA was solubilized in RNase-free water, and first-strand cDNA was generated starting from 1 μg of total RNA using the GoScript Reverse Transcription System (Promega Italia). In order to hybridize to unique regions of the appropriate gene sequence, specific sets of primer pairs were designed and tested with primer-BLAST (NCBI, see list in Table 1). Real-time PCR was performed using the iTAQ universal SYBR Green Supermix (Bio-Rad Laboratories) on a StepOne real-time PCR System (Life-Technologies). All reactions were run in triplicate. Resulting data were analyzed by the StepOne™ Software (v2.3) using the second-derivative maximum method. The fold changes in mRNA levels were determined relative to a control after normalizing to the internal standard HPRT.

Statistical analyses

Values are expressed as means ± SEM (except for those relative to densitometric analyses that are expressed as mean ± SD). The statistical significance of the differences between means was assessed by an independent Student's *t*-test in order to determine which groups differed significantly from the others. A probability of 0.05% ($p = 0.05$) was considered significant.

Acknowledgments

G.F. is supported by grants from the National Ministry of Health, Young Italian Researcher Grant-2008 (Grant GR-2008-1138121), and from the Italian Association for Cancer Research, AIRC-MFAG 2011 (Grant 11452). P.B. is supported by grants from Telethon-Italy (Grant GGP10225) and the Italian Ministry of Education, University, and Research (Grant RBAP11Z3YA_003).

The authors gratefully acknowledge Jonathan S. Stamler for having kindly provided GSNOR-KO mice; Elena

Romano for her technical assistance in fluorescence microscopy and image analyses; Stefania Gonfloni, Silvia Consalvi, and Claudia Cirotti for experimental advice and lab assistance; Silvia Castagnaro and Martina Chrisam for help during treadmill experiments; Walter Giuriati for assistance with electron microscopy; and Søs Grønbæk Mathiassen for a critical reading of the article and fruitful discussions.

Author Disclosure Statement

The authors state that no competing financial interests exist.

References

1. Allaire J, Maltais F, LeBlanc P, Simard PM, Whittom F, Doyon JF, Simard C, and Jobin J. Lipofuscin accumulation in the vastus lateralis muscle in patients with chronic obstructive pulmonary disease. *Muscle Nerve* 25: 383–389, 2002.
2. Altamirano F, López JR, Henríquez C, Molinski T, Allen PD, and Jaimovich E. Increased resting intracellular calcium modulates NF-κB-dependent inducible nitric-oxide synthase gene expression in dystrophic mdx skeletal myotubes. *J Biol Chem* 287: 20876–20887, 2012.
3. Andersson DC, Betzenhauser MJ, Reiken S, Meli AC, Umanskaya A, Xie W, Shiomi T, Zalk R, Lacampagne A, and Marks AR. Ryanodine receptor oxidation causes intracellular calcium leak and muscle weakness in aging. *Cell Metab* 14: 196–207, 2011.
4. Barreiro E, Comtois AS, Gea J, Laubach VE, and Hussain SN. Protein tyrosine nitration in the ventilatory muscles: role of nitric oxide synthases. *Am J Respir Cell Mol Biol* 26: 438–446, 2002.
5. Beal MF, Ferrante RJ, Browne SE, Matthews RT, Kowall NW, and Brown RH Jr. Increased 3-nitrotyrosine in both sporadic and familial amyotrophic lateral sclerosis. *Ann Neurol* 42: 644–654, 1997.
6. Beckman JS and Koppenol WH. Nitric oxide, superoxide, and peroxynitrite: the good, the bad, and ugly *Am J Physiol* 271: C1424–C1437, 1996.
7. Beckman JS. Oxidative damage and tyrosine nitration from peroxynitrite. *Chem Res Toxicol* 9: 836–844, 1996.
8. Bellinger AM, Reiken S, Carlson C, Mongillo M, Liu X, Rothman L, Matecki S, Lacampagne A, and Marks AR. Hypernitrosylated ryanodine receptor calcium release channels are leaky in dystrophic muscle. *Nat Med* 15: 325–330, 2009.
9. Benhar M, Forrester MT, and Stamler JS. Protein denitrosylation: enzymatic mechanisms and cellular functions. *Nat Rev Mol Cell Biol* 10: 721–732, 2009.
10. Bernabucci M, Notartomaso S, Zappulla C, Fazio F, Cannella M, Motolese M, Battaglia G, Bruno V, Gradini R, and Nicoletti F. *N*-Acetyl-cysteine causes analgesia by reinforcing the endogenous activation of type-2 metabotropic glutamate receptors. *Mol Pain* 8: 77, 2012.
11. Cereghetti GM, Stangherlin A, Martins de Brito O, Chang CR, Blackstone C, Bernardi P, and Scorrano L. Dephosphorylation by calcineurin regulates translocation of Drp1 to mitochondria. *Proc Natl Acad Sci U S A* 105: 15803–15808, 2008.
12. Choe MA and An GJ. Effects of nitric oxide synthase inhibitor on hindlimb muscles in rats with neuropathic pain induced by unilateral peripheral nerve injury. *J Korean Acad Nurs* 41: 520–527, 2011.
13. Colussi C, Mozzetta C, Gurtner A, Illi B, Rosati J, Straino S, Ragone G, Pescatori M, Zaccagnini G, Antonini A, Minetti G, Martelli F, Piaggio G, Gallinari P, Steinkuhler C, Clementi E, Dell'Aversana C, Altucci L, Mai A, Capogrossi MC, Puri PL, and Gaetano C. HDAC2 blockade by nitric oxide and histone deacetylase inhibitors reveals a common target in Duchenne muscular dystrophy treatment. *Proc Natl Acad Sci U S A* 105: 19183–19187, 2008.
14. Cox AG, Saunders DC, Kelsey PB Jr, Conway AA, Tesmenitsky Y, Marchini JF, Brown KK, Stamler JS, Colagiovanni DB, Rosenthal GJ, Croce KJ, North TE, and Goessling W. S-nitrosothiol signaling regulates liver development and improves outcome following toxic liver injury. *Cell Rep* 6: 56–69, 2014.
15. Di Giacomo G, Rizza S, Montagna C, and Filomeni G. Established principles and emerging concepts on the interplay between mitochondrial physiology and S-(de)nitrosylation: Implications in cancer and neurodegeneration. *Int J Cell Biol* 2012: 361872, 2012.
16. Dixon WJ. Efficient analysis of experimental observations. *Annu Rev Pharmacol Toxicol* 20: 441–462, 1980.
17. Doyle T, Chen Z, Muscoli C, Bryant L, Esposito E, Cuzzocrea S, Dagostino C, Ryerse J, Rausaria S, Kamadulski A, Neumann WL, and Salvemini D. Targeting the overproduction of peroxynitrite for the prevention and reversal of paclitaxel-induced neuropathic pain. *J Neurosci* 32: 6149–6160, 2012.
18. Dudley RW, Danialou G, Govindaraju K, Lands L, Eidelman DE, and Petrof BJ. Sarcolemmal damage in dystrophin deficiency is modulated by synergistic interactions between mechanical and oxidative/nitrosative stresses. *Am J Pathol* 168: 1276–1287, 2006.
19. Filomeni G, Cerchiaro G, Da Costa Ferreira AM, De Martino A, Pedersen JZ, Rotilio G, and Ciriolo MR. Pro-apoptotic activity of novel Isatin-Schiff base copper(II) complexes depends on oxidative stress induction and organelle-selective damage. *J Biol Chem* 282: 12010–12021, 2007.
20. Forrester MT, Foster MW, Benhar M, and Stamler JS. Detection of protein S-nitrosylation with the biotin-switch technique. *Free Radic Biol Med* 46: 119–126, 2009.
21. Foster MW, Hess DT, and Stamler JS. Protein *S*-nitrosylation in health and disease: a current perspective. *Trends Mol Med* 15: 391–404, 2009.
22. Grumati P, Coletto L, Sabatelli P, Cescon M, Angelin A, Bertaggia E, Blaauw B, Urciuolo A, Tiepolo T, Merlini L, Maraldi NM, Bernardi P, Sandri M, and Bonaldo P. Autophagy is defective in collagen VI muscular dystrophies, and its reactivation rescues myofiber degeneration. *Nat Med* 16: 1313–1320, 2010.
23. Grumati P, Coletto L, Schiavinato A, Castagnaro S, Bertaggia E, Sandri M, and Bonaldo P. Physical exercise stimulates autophagy in normal skeletal muscles but is detrimental for collagen VI-deficient muscles. *Autophagy* 7: 1415–1423, 2011.
24. Hall DT, Ma JF, Marco SD, and Gallouzi IE. Inducible nitric oxide synthase (iNOS) in muscle wasting syndrome, sarcopenia, and cachexia. *Aging* 3: 702–715, 2011.
25. He C, Bassik MC, Moresi V, Sun K, Wei Y, Zou Z, An Z, Loh J, Fisher J, Sun Q, Korsmeyer S, Packer M, May HI, Hill JA, Virgin HW, Gilpin C, Xiao G, Bassel-Duby R, Scherer PE, and Levine B. Exercise-induced BCL2-regulated autophagy is required for muscle glucose homeostasis. *Nature* 481: 511–515, 2012.
26. Ischiropoulos H. Protein tyrosine nitration-an update. *Arch Biochem Biophys* 484: 117–121, 2009.

27. Kamei J, Tamura N, and Saitoh A. Possible involvement of the spinal nitric oxide/cGMP pathway in vincristine-induced painful neuropathy in mice. *Pain* 117: 112–120, 2005.
28. Kaneki M, Shimizu N, Yamada D, and Chang K. Nitrosative stress and pathogenesis of insulin resistance. *Antioxid Redox Signal* 9: 319–329, 2007.
29. Kohn RR. Denervation muscle atrophy: an autolytic system *in vitro*. *Am J Pathol* 47: 315–323, 1965.
30. Kwon J, Han E, Bui CB, Shin W, Lee J, Lee S, Choi YB, Lee AH, Lee KH, Park C, Obin MS, Park SK, Seo YJ, Oh GT, Lee HW, and Shin J. Assurance of mitochondrial integrity and mammalian longevity by the p62-Keap1-Nrf2-Nqo1 cascade. *EMBO Rep* 13:150–156, 2012.
31. Lau A, Wang XJ, Zhao F, Villeneuve NF, Wu T, Jiang T, Sun Z, White E, and Zhang DD. A noncanonical mechanism of Nrf2 activation by autophagy deficiency: direct interaction between Keap1 and p62. *Mol Cell Biol* 30: 3275–3285, 2010.
32. Lehmann HC, Köhne A, Meyer zu Hörste G, Dehmel T, Kiehl O, Hartung HP, Kastenbauer S, and Kieseier BC. Role of nitric oxide as mediator of nerve injury in inflammatory neuropathies. *J Neuropathol Exp Neurol* 66: 305–312, 2007.
33. Li D, Shin JH, and Duan D. iNOS ablation does not improve specific force of the extensor digitorum longus muscle in dystrophin-deficient mdx4cv mice. *PLoS One* 6: e21618, 2011.
34. Li D, Yue Y, Lai Y, Hakim CH, and Duan D. Nitrosative stress elicited by nNOSμ delocalization inhibits muscle force in dystrophin-null mice. *J Pathol* 223: 88–98, 2011.
35. Liu L, Hausladen A, Zeng M, Que L, Heitman J, and Stamler JS. A metabolic enzyme for S-nitrosothiol conserved from bacteria to humans. *Nature* 410: 490–494, 2001.
36. Liu L, Yan Y, Zeng M, Zhang J, Hanes MA, Ahearn G, McMahon TJ, Dickfeld T, Marshall HE, Que LG, and Stamler JS. Essential roles of S-nitrosothiols in vascular homeostasis and endotoxic shock. *Cell* 116: 617–628, 2004.
37. Mangiarini L, Sathasivam K, Seller M, Cozens B, Harper A, Hetherington C, Lawton M, Trottier Y, Lehrach H, Davies SW, and Bates GP. Exon 1 of an expanded CAG repeat is sufficient to cause a progressive neurological phenotype in transgenic mice. *Cell* 87: 493–560, 1996.
38. Martínez-Ruiz A, Cadenas S, and Lamas S. Nitric oxide signaling: classical, less classical, and nonclassical mechanisms. *Free Radic Biol Med* 51: 17–29, 2011.
39. Mizushima N and Kuma A. Autophagosomes in GFP-LC3 Transgenic Mice. *Methods Mol Biol* 445: 119–124, 2008.
40. Moncada S and Erusalimsky JD. Does nitric oxide modulate mitochondrial energy generation and apoptosis? *Nat Rev Mol Cell Biol* 3: 214–220, 2002.
41. Murakami H, Guillet C, Tardif N, Salles J, Migné C, Boirie Y, and Walrand S. Cumulative 3-nitrotyrosine in specific muscle proteins is associated with muscle loss during aging. *Exp Gerontol* 47: 129–135, 2012.
42. Nakamura T and Lipton SA. Redox modulation by S-nitrosylation contributes to protein misfolding, mitochondrial dynamics, and neuronal synaptic damage in neurodegenerative diseases. *Cell Death Differ* 18: 1478–1486, 2011.
43. Pacher P, Obrosova IG, Mabley JG, and Szabó C. Role of nitrosative stress and peroxynitrite in the pathogenesis of diabetic complications. Emerging new therapeutical strategies. *Curr Med Chem* 12: 267–275, 2005.
44. Palacios D, Mozzetta C, Consalvi S, Caretti G, Saccone V, Proserpio V, Marquez VE, Valente S, Mai A, Forcales SV, Sartorelli V, and Puri PL. TNF/p38α/polycomb signaling to Pax7 locus in satellite cells links inflammation to the epigenetic control of muscle regeneration. *Cell Stem Cell* 7: 455–469, 2010.
45. Pasinelli P and Brown RH. Molecular biology of amyotrophic lateral sclerosis: insights from genetics. *Nat Rev Neurosci* 9: 710–723, 2006.
46. Pattison JS, Osinska H, and Robbins J. Atg7 induces basal autophagy and rescues autophagic deficiency in CryABR120G cardiomyocytes. *Circ Res* 109: 151–160, 2011.
47. Piantadosi CA. Regulation of mitochondrial processes by protein S-nitrosylation. *Biochim Biophys Acta* 1820: 712–721, 2011.
48. Price SR, Bailey JL, Wang X, Jurkovitz C, England BK, Ding X, Phillips LS, and Mitch WE. Muscle wasting in insulinopenic rats results from activation of the ATP-dependent, ubiquitin-proteasome proteolytic pathway by a mechanism including gene transcription. *J Clin Invest* 98: 1703–1708, 1996.
49. Rafuse VF and Gordon T. Incomplete rematching of nerve and muscle properties in motor units after extensive nerve injuries in cat hindlimb muscle. *J Physiol* 509: 909–926, 1998.
50. Ramachandran J, Schneider JS, Crassous PA, Zheng R, Gonzalez JP, Xie LH, Beuve A, Fraidenraich D, and Peluffo RD. Nitric oxide signalling pathway in Duchenne muscolar dystrophy mice: up-regulation of L-arginine transporters. *Biochem J* 449: 133–142, 2013.
51. Reid MB, Stokić DS, Koch SM, Khawli FA, and Leis AA. N-acetylcysteine inhibits muscle fatigue in humans. *J Clin Invest* 94: 2468–2474, 1994.
52. Romanello V, Guadagnin E, Gomes L, Roder I, Sandri C, Petersen Y, Milan G, Masiero E, Del Piccolo P, Foretz M, Scorrano L, Rudolf R, and Sandri M. Mitochondrial fission and remodelling contributes to muscle atrophy. *EMBO J* 29: 1774–1785, 2010.
53. Sarkar S, Korolchuk VI, Renna M, Imarisio S, Fleming A, Williams A, Garcia-Arencibia M, Rose C, Luo S, Underwood BR, Kroemer G, O'Kane CJ, and Rubinsztein DC. Complex inhibitory effects of nitric oxide on autophagy *Mol Cell* 43:19–32, 2011.
54. Smith LW, Smith JD, and Criswell DS. Involvement of nitric oxide synthase in skeletal muscle adaptation to chronic overload. *J Appl Physiol* 92: 2005–2011, 2002.
55. Souza JM, Peluffo G, and Radi R. Protein tyrosine nitration: functional alteration or just a biomarker? *Free Radic Biol Med* 45: 357–366, 2008.
56. Stamler JS and Meissner G. Physiology of nitric oxide in skeletal muscle. *Physiol Rev* 81: 209–237, 2001.
57. Stamler JS, Sun QA, and Hess DT. A SNO storm in skeletal muscle. *Cell* 133: 33–35, 2008.
58. Stauber WT, Bird JW, and Schottelius BA. Catalase: an enzymatic indicator of the degree of muscle wasting. *Exp Neurol* 55: 381–389, 1977.
59. Suhr F, Gehlert S, Grau M, and Bloch W. Skeletal Muscle Function during Exercise-Fine-Tuning of Diverse Subsystems by Nitric Oxide. *Int J Mol Sci* 14: 7109–7139, 2013.
60. Sun J, Xin C, Eu JP, Stamler JS, and Meissner G. Cysteine-3635 is responsible for skeletal muscle ryanodine receptor modulation by NO. *Proc Natl Acad Sci U S A* 98: 11158–11162, 2001.
61. Suzuki N, Motohashi N, Uezumi A, Fukada S, Yoshimura T, Itoyama Y, Aoki M, Miyagoe-Suzuki Y, and Takeda S. NO production results in suspension-induced muscle

atrophy through dislocation of neuronal NOS. *J Clin Invest* 117: 2468–2476, 2007.
62. Wakabayashi K, Mori F, Tanji K, Orimo S, and Takahashi H. Involvement of the peripheral nervous system in synucleinopathies, tauopathies and other neurodegenerative proteinopathies of the brain. *Acta Neuropathol* 120: 1–12, 2010.
63. Wang X, Kettenhofen NJ, Shiva S, Hogg N, and Gladwin MT. Copper dependence of the biotin switch assay: modified assay for measuring cellular and blood nitrosated proteins. *Free Radic Biol Med* 44: 1362–1372, 2008.
64. Wei W, Li B, Hanes MA, Kakar S, Chen X, and Liu L. *S*-nitrosylation from GSNOR deficiency impairs DNA repair and promotes hepatocarcinogenesis. *Sci Transl Med* 2: 19ra13, 2010.
65. Wells KE, Torelli S, Lu Q, Brown SC, Partridge T, Muntoni F, and Wells DJ. Relocalization of neuronal nitric oxide synthase (nNOS) as a marker for complete restoration of the dystrophin associated protein complex in skeletal muscle. *Neuromuscul Disord* 13: 21–31, 2003.
66. Wu M, Katta A, Gadde MK, Liu H, Kakarla SK, Fannin J, Paturi S, Arvapalli RK, Rice KM, Wang Y, and Blough ER. Aging-associated dysfunction of Akt/protein kinase B: S-nitrosylation and acetaminophen intervention. *PLoS One* 4: e6430, 2009.

Address correspondence to:
Dr. Giuseppe Filomeni
Department of Biology
University of Rome ''Tor Vergata''
Via della Ricerca Scientifica
Rome 00133
Italy

E-mail: filomeni@bio.uniroma2.it
giufil@cancer.dk

Date of first submission to ARS Central, October 23, 2013; date of final revised submission, March 12, 2014; date of acceptance, March 29, 2014.

Abbreviations Used

α-SG = α-Sarcoglycan
$\Delta\psi_m$ = transmembrane potential
AMPK = AMP-dependent protein kinase
Atg7 = autophagy gene 7
Bnip3 = BCL2/adenovirus E1B 19 kd-interacting protein 3
Col6a1 = collagen VI
CSA = cross-sectional area
CTX = cardiotoxin
DNP = dinitrophenylhydrazine
eNOS = endothelial NOS
FoxO = Forkhead box O
GFP = green fluorescent protein
GSNO = *S*-nitrosoglutathione
GSNOR = *S*-nitrosoglutathione reductase
HCC = hepatocellular carcinoma
HRP = horseradish peroxidase
IKKβ = inhibitor of NF-κB kinase β
iNOS = inducible NOS
Keap1 = Kelch-like ECH-associated protein 1
LC3B = microtubule-associated protein 1 light chain 3B
LDH = lactate dehydrogenase
Mdx = *dystrophin-null*
MEFs = mouse embryonic fibroblasts
MyHC = slow myosin heavy chain
NAC = *N*-acetylcysteine
nNOS = neuronal nitric oxide synthase
NO = nitric oxide
Nqo1 = NAD(P)H:quinone oxidoreductase 1
Nrf2 = nuclear factor (erythroid-derived 2)-like 2
Opa1 = optic atrophy protein 1
PARP1 = polyADP-ribose polymerase 1,
PSNOs = protein nitrosothiols
RNS = reactive nitrogen species
ROS = reactive oxygen species
RyR1 = ryanodine receptor 1
SNO = *S*-nitrosothiol
Sod = superoxide dismutase
SQSTM1 = sequestrosoma 1
Trx1 = thioredoxin 1